

The Effects of Varying the Timing of Inputs on a Neural Oscillator*

Christina Ambrosio-Mouser[†], Farzan Nadim[‡], and Amitabha Bose[§]

Abstract. The gastric mill network of the crab *Cancer borealis* is an oscillatory neural network with frequency ~ 0.1 Hz. Oscillations in this network require neuromodulatory synaptic inputs as well as rhythmic inputs from the faster (~ 1 Hz) pyloric neural oscillator. We study how the frequency of the gastric mill network is determined when it receives rhythmic input from two different sources but where the timing of these inputs may differ. We find that over a certain range of the time difference one of the two rhythmic inputs plays no role what so ever in determining the network frequency, while in another range, both inputs work together to determine the frequency. The existence and stability of periodic solutions to model sets of equations are obtained analytically using geometric singular perturbation theory. The results are validated through numerical simulations. Comparisons to experiments are also presented.

Key words. synapse, stomatogastric ganglion, periodic orbit, Poincaré map

AMS subject classifications. 34A26, 37C25, 92B05

DOI. 10.1137/050625795

1. Introduction. Many rhythmically active biological systems require input from extrinsic sources to produce their activity. Such extrinsic inputs may arrive as a trigger signal thereby switching on the oscillation, or be continuously present as forcing or feedback for the duration of the oscillation [17, 18, 27]. The extrinsic input itself is often rhythmic and its frequency may or may not match that of the target oscillator. Often, the oscillating network receives multiple inputs simultaneously—for example, a central command input and a sensory feedback input. Such inputs are readily identified in central pattern generators (CPGs), neural networks within the central nervous system (CNS) that are responsible for generating rhythmic motor behaviors such as locomotion, swimming, or breathing [13, 15, 17]. However, even in cases where the extrinsic inputs to a biological oscillator are known, the significance of the rhythmicity of such inputs or the consequences of having multiple inputs is largely unknown; often a nonrhythmic (tonic) input or only one of multiple inputs is sufficient to produce the biological oscillation. For instance, the CPG responsible for swimming in lower species of fish consists of chains of oscillators in the spinal cord [14]. This CPG receives rhythmic command input from the brain as well as multiple rhythmic and tonic sensory feedback inputs from the body. Without these inputs the CPG is inactive and the animal does not swim. However, the

*Received by the editors March 2, 2005; accepted for publication (in revised form) by D. Terman October 12, 2005; published electronically February 14, 2006. This work was supported in part by the National Science Foundation DMS-0315862 (AB, CA) and the National Institutes of Health MH-60605 (FN).

<http://www.siam.org/journals/siads/5-1/62579.html>

[†]Department of Mathematics, Medgar Evers College, Brooklyn, NY 11225 and Department of Mathematical Sciences, New Jersey Institute of Technology, Newark, NJ 07102 (cmouser@mec.cuny.edu).

[‡]Department of Mathematical Sciences, New Jersey Institute of Technology, Newark, NJ 07102 and Department of Biological Sciences, Rutgers University at Newark, Newark, NJ 07102 (farzan@njit.edu).

[§]Department of Mathematical Sciences, New Jersey Institute of Technology, Newark, NJ 07102 (bose@njit.edu).

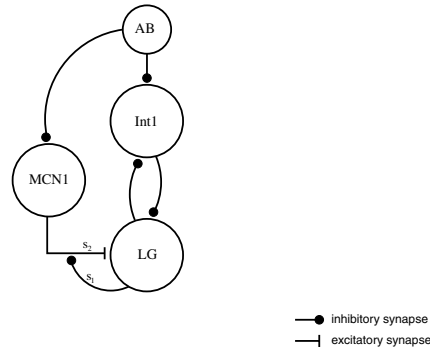


Figure 1. *Synaptic architecture of neurons associated with the gastric mill rhythm.*

isolated spinal cord, in the presence of a chemical stimulant (tonic input) produces “fictive swimming,” rhythmic patterns which appear identical to those responsible for swimming in the intact animal [12].

In this paper, we use mathematical analysis to investigate the significance of the timing of multiple inputs to a biological oscillator. We focus on the rhythmically active crustacean gastric mill CPG located within the stomatogastric ganglion (STG). The STG is one of several ganglia in the crustacean CNS that control feeding and digestion behaviors [24]. As in many invertebrate systems, the small number of neurons in the STG makes it amenable to both experimental and modeling studies of neuronal networks responsible for generating behaviors.

The gastric mill rhythm is generated by a subset of neurons in the STG. At the heart of this rhythm are two neurons, lateral gastric (*LG*) and interneuron 1 (*Int1*), which make reciprocally inhibitory synaptic connections and (when the gastric mill rhythm is activated) oscillate in antiphase with a frequency of 0.1 Hz (see Figure 1). The gastric mill CPG, however, is a conditional oscillator; its activity depends on (modulatory) input from central command neurons located in other CNS ganglia [18, 24]. One such neuron, the modulatory commissural neuron 1 (*MCN1*), when excited, elicits a sustained gastric mill rhythm [8]. Previous studies have shown that input from the much faster pyloric CPG (frequency 1 Hz; also located in the STG) is crucial in setting the frequency of the *MCN1*-elicited gastric mill rhythm [3, 21]. This input comes in the form of an inhibitory synapse to *Int1* from the pyloric pacemaker neuron anterior burster (*AB*). Although tonic excitation of *MCN1* is sufficient for eliciting a gastric mill rhythm [3], it is known that, in the intact CNS, *MCN1* is itself rhythmically active [30]. The rhythmicity of *MCN1* is also due to a synaptic input it receives from *AB*. Thus, there are two pathways by which the pyloric pacemaker neuron *AB* influences the gastric mill network: the direct synaptic connection from *AB* to *Int1* and the indirect synaptic influence exerted by inhibiting *MCN1* which, in turn, excites the gastric mill neurons. Recent experimental findings show that the presence of either or both of the two pathways of *AB* influences results in a gastric mill rhythm of similar frequency [30]. However, when both pathways are removed (and thus the *MCN1* activity is tonic) the gastric mill rhythm slows down significantly. Although the mechanism through which the direct pyloric input influences the gastric mill frequency is understood, it is not known how the rhythmic activity of *MCN1* provides an apparently redundant mechanism for maintaining the gastric

mill frequency.

We expand on the techniques of Manor et al. [16] and build a simplified, biophysically based model of the gastric mill network incorporating the effects of both *MCN1* and *AB*. Using this model, we show that the time difference between the two distinct *AB* influences on the gastric mill is critical in determining the gastric mill frequency. When m , the time delay between the *AB* inhibition of *Int1* and *MCN1*, is small, the gastric mill frequency is determined solely by direct modulatory effects of *MCN1* on the gastric mill neurons. However, when m is large, the gastric mill rhythm operates at a higher frequency and is determined by both the *MCN1* and *AB* inputs. Throughout this work, we use geometric singular perturbation theory to examine the behavior of our model on low-dimensional manifolds. We also use phase plane analysis as a means of geometrically understanding the behavior of the network. Using these mathematical tools, we prove the existence and stability of periodic solutions of the model when the activity of *MCN1* is either tonic or rhythmic. Furthermore, we confirm our findings through numerical simulations in which we change the delay parameter m and numerically calculate the period. We then compare our results with the experimental findings of [30]. The results from our model match the experimental results only when m is either 0 or small. We note that in the work of Wood et al., the delay between the pyloric and modulatory inputs is never explicitly measured. Our analysis, therefore, gives a possible explanation for the experimental results. The findings could be tested in future experiments by artificially introducing different delays between the timing of the modulatory and pyloric inputs to the gastric mill network and determining the effect on the gastric mill rhythm frequency.

The remainder of the paper is organized as follows. In section 2, we derive a model set of equations and show how it can be reduced into sets of fast and slow equations. The effect of various synaptic inputs on relevant nullclines are illustrated with the goal of showing how fixed points of the fast set of equations depend on these inputs. In section 3, we prove the existence, uniqueness, and stability of periodic solutions for four different cases of the gastric mill rhythm. These cases are considered so that we may parallel the study of Wood et al. [30]. In section 4, we derive an analytic formula for the period of the solutions for the four different cases. We then check our analytic results against simulations. In section 5, we discuss the impact of making a certain synapse (that from *MCN1* to *LG*) voltage dependent. Section 6 contains a discussion to conclude the paper.

2. Model. Our model consists of the gastric mill network composed of *Int1* and *LG*, the pacemaker neuron *AB* of the pyloric network, and the modulatory commissural neuron *MCN1*; see Figure 1. *LG* and *Int1* are modeled as passive neurons (*LG* having a subthreshold resting potential and *Int1* having a suprathreshold resting potential). In the absence of *AB* input, *MCN1* is tonically active. Therefore, we also model *MCN1* as a passive neuron with a suprathreshold resting potential. *LG* and *Int1* have reciprocally inhibitory synapses between them. *Int1* and *MCN1* receive inhibitory input from the pacemaker neuron *AB*. *AB* and *MCN1* both fire in pyloric time with a period denoted P_{AB} . *AB* sends an inhibitory synapse to *Int1*. *MCN1* sends a slow excitatory synapse to *LG*. In addition, *LG* presynaptically inhibits *MCN1* each time it fires, thus removing the excitation from *MCN1* to *LG*. Through this circuitry, the voltage of *LG* is able to increase above threshold (due to the excitation it receives from *MCN1*), causing *Int1* to become suppressed, and then decay back below

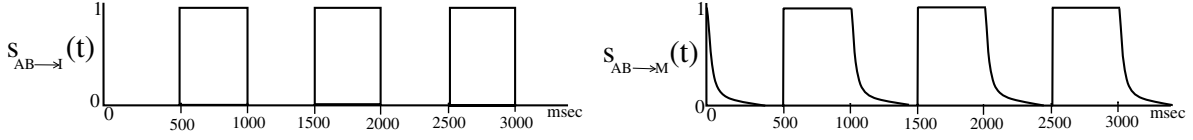


Figure 2. The synaptic variables $s_{AB \rightarrow I}(t)$ and $s_{AB \rightarrow M}(t)$. Note that $s_{AB \rightarrow M}(t)$ decays with time constant τ_{AB} .

threshold (due to the presynaptic inhibition), thereby producing the antiphase oscillations of the gastric mill rhythm [9, 16].

2.1. Equations. We do not explicitly model the pacemaker neuron AB but instead incorporate its effect on $MCN1$ and $Int1$ through the synaptic variables $s_{AB \rightarrow I}(t)$ and $s_{AB \rightarrow M}(t)$. $s_{AB \rightarrow I}(t)$ is a square wave with amplitude 1 and period, P_{AB} , which has experimentally been found to be approximately 1 sec. Let D_c denote the duty cycle of AB (the ratio of its active time to its period). During one period of AB , the variable $s_{AB \rightarrow I}$ is equal to 1 for a time $D_c P_{AB}$ and equal to 0 for a time $P_{AB}[1 - D_c]$. $s_{AB \rightarrow M}(t)$ is similar in form to $s_{AB \rightarrow I}(t)$ in that $s_{AB \rightarrow M}$ oscillates between 0 and 1. The jump in $s_{AB \rightarrow M}$ from 0 to 1 is instantaneous. However, $s_{AB \rightarrow M}$ decreases from 1 to 0 with time constant τ_{AB} (see Figure 2).

The dynamics of the system evolve along two distinct timescales. One is a slow timescale corresponding to the effect of presynaptic inhibition from LG to the slow excitatory component of the $MCN1$ synapse. The other is a fast timescale along which all other synapses and intrinsic properties evolve. We use a small parameter, ϵ , to demarcate these two timescales.

The equations to describe the activity of LG , $Int1$, and $MCN1$ are

(1)

$$\epsilon \frac{dV_L}{dt} = -g_{leak,L}[V_L - E_{leak,L}] - \bar{g}_{I \rightarrow L} n_\infty(V_I)[V_L - E_{I \rightarrow L}] - g_s(V_L)s(t)[V_L - E_{exc}],$$

(2)

$$\epsilon \frac{dV_I}{dt} = -g_{leak,I}[V_I - E_{leak,I}] - \bar{g}_{L \rightarrow I} n_\infty(V_L)[V_I - E_{L \rightarrow I}] - \bar{g}_{AB \rightarrow I} s_{AB \rightarrow I}(t)[V_I - E_{AB \rightarrow I}],$$

(3)

$$\epsilon \frac{dV_M}{dt} = -g_{leak,M}[V_M - E_{leak,M}] - \bar{g}_{AB \rightarrow M} s_{AB \rightarrow M}(t)[V_M - E_{AB \rightarrow M}],$$

where V_L is the voltage of LG , V_I is the voltage of $Int1$, and V_M is the voltage of $MCN1$. $g_{leak,L}$, $g_{leak,I}$, and $g_{leak,M}$ are the conductances of the leak currents in LG , $Int1$, and $MCN1$. $E_{leak,L}$, $E_{leak,I}$, and $E_{leak,M}$ are the reversal potentials of the leak currents in LG , $Int1$, and $MCN1$. Denote the right-hand sides of (1) and (2) by $f(V_L, V_I, s)$ and $g(V_I, V_L, s_{AB \rightarrow I})$, respectively.

The parameters of the reciprocally inhibitory synapses between $Int1$ and LG are $\bar{g}_{I \rightarrow L}$ and $\bar{g}_{L \rightarrow I}$ (the maximal conductances) and $E_{I \rightarrow L}$ and $E_{L \rightarrow I}$ (the reversal potentials). $n_\infty(V_I)$ and $n_\infty(V_L)$ are sigmoidally shaped gating functions lying between 0 and 1:

$$(4) \quad n_\infty(V_x) = \left(1 + \exp \frac{v_x - V_x}{k_x} \right)^{-1},$$

where v_x is the half-activation voltage and k_x is inversely related to the slope at this point.

The fast, periodic inhibitory input from AB to $MCN1$ is described by $\bar{g}_{AB \rightarrow M} s_{AB \rightarrow M}(t)[V_M - E_{AB \rightarrow M}]$, where $\bar{g}_{AB \rightarrow M}$ is the conductance of the synapse and $E_{AB \rightarrow M}$ is the reversal potential which is chosen to be less than $E_{leak, M}$ so that the input from AB to $MCN1$ is inhibitory. The equation to describe the activity of $s_{AB \rightarrow M}(t)$ with respect to AB is

$$(5) \quad \epsilon \frac{ds_{AB \rightarrow M}}{dt} = \begin{cases} [1 - s_{AB \rightarrow M}]/\tau_{M1}, & V_{AB} \geq V_{Th(AB)}, \\ -\epsilon s_{AB \rightarrow M}/\tau_{M2}, & V_{AB} < V_{Th(AB)}, \end{cases}$$

where V_{AB} is a square wave with period P_{AB} and duty cycle $= D_c$. Thus, when $s_{AB \rightarrow M} = 0$, V_M lies at a maximum voltage of $E_{leak, M}$. When $s_{AB \rightarrow M} = 1$, V_M lies at a minimum voltage of V_M^* , where

$$(6) \quad V_M^* = \frac{g_{leak, M} E_{leak, M} + \bar{g}_{AB \rightarrow M} E_{AB \rightarrow M}}{g_{leak, M} + \bar{g}_{AB \rightarrow M}}.$$

The periodic, inhibitory input from AB to $Int1$ is given by $\bar{g}_{AB \rightarrow I} s_{AB \rightarrow I}(t)[V_I - E_{AB \rightarrow I}]$. $\bar{g}_{AB \rightarrow I}$ is the conductance and $E_{AB \rightarrow I}$ is the reversal potential. An important aspect of this work is to highlight the fact that different timing relationships of AB input to $MCN1$ and $Int1$ lead to dramatically different frequencies of the gastric mill rhythm. To this end, we will use the parameter, m , to delay the AB input to $Int1$ relative to $MCN1$. In other words, if the AB input to $MCN1$ turns on at $t = 0$, the input from AB to $Int1$ does not turn on until $t = m$. The parameter m is a constant which can range between 0 and P_{AB} (the period of AB).

The effect of the excitation that LG receives from $MCN1$ is given in (1) by $g_s(V_L)s(t)[V_L - E_{exc}]$, where $g_s(V_L) = \bar{g}_s s_\infty(V_L)$ is the voltage dependent conductance of the synapse, E_{exc} is the reversal potential, and $s(t)$ models the amount of excitation LG receives. The function s_∞ is a sigmoidal gating function similar in form to n_∞ ; its exact form will be discussed later in section 5. We express $s(t) = s_1(t)s_2(t)$ as the product of two different effects. $s_1(t)$ models the effect of the presynaptic inhibition of the slow excitatory component of the $MCN1$ to LG synapse. $s_2(t)$ models the effect of the AB inhibition of $MCN1$ on the fast excitatory component of the $MCN1$ to LG synapse. The relevant equations are

$$(7) \quad \frac{ds_1}{dt} = \begin{cases} [1 - s_1]/\tau_{r1}, & V_L \leq V_T, \\ -s_1/\tau_{f1}, & V_L > V_T, \end{cases}$$

$$(8) \quad \epsilon \frac{ds_2}{dt} = \begin{cases} [1 - s_2]/\tau_{r2}, & V_M \geq V_{Th(M)}, \\ [s_{2min} - s_2]/\tau_{f2}, & V_M < V_{Th(M)}. \end{cases}$$

The time constants τ_{M1} , τ_{M2} , τ_{r1} , τ_{f1} , τ_{r2} , and τ_{f2} in (5), (7), and (8) are $O(1)$ with respect to ϵ . When V_L goes above threshold, the presynaptic inhibition turns on, which causes $s_1(t)$ to decrease on the slow timescale. When V_L goes below threshold, the presynaptic inhibition turns off, which causes $s_1(t)$ to increase on the slow timescale (see Figure 1). When $MCN1$ is inhibited by AB , s_2 decreases on the fast timescale. Once the inhibition from AB is removed, s_2 increases on the fast timescale. The parameters $V_{Th(M)}$ and V_T denote the activation thresholds for these two synapses.

To understand which parameters are important in controlling the gastric mill frequency, we use phase plane analysis along with geometric singular perturbation theory to reduce the full flow to a study of flow on lower-dimensional slow manifolds. From (1)–(3) and (7)–(8), we see that V_L , V_I , V_M , and s_2 evolve on a faster timescale than s_1 . Setting $\epsilon = 0$ in the equations yields the slow equations

$$\begin{aligned}
(9) \quad & 0 = f(V_L, V_I, s), \\
(10) \quad & 0 = g(V_I, V_L, s_{AB \rightarrow I}), \\
(11) \quad & 0 = -g_{leak, M}[V_M - E_{leak, M}] - \bar{g}_{AB \rightarrow M} s_{AB \rightarrow M}(t)[V_M - E_{AB \rightarrow M}], \\
(12) \quad & 0 = [1 - s_{AB \rightarrow M}]/\tau_{M1}, \quad V_{AB} \geq V_{Th(AB)}, \\
(13) \quad & \frac{ds_{AB \rightarrow M}}{dt} = -s_{AB \rightarrow M}/\tau_{M2}, \quad V_{AB} < V_{Th(AB)}, \\
(14) \quad & \frac{ds_1}{dt} = \begin{cases} [1 - s_1]/\tau_{r1}, & V_L \leq V_T, \\ -s_1/\tau_{f1}, & V_L > V_T, \end{cases} \\
(15) \quad & 0 = \begin{cases} [1 - s_2]/\tau_{r2}, & V_M \geq V_{Th(M)}, \\ [s_{2min} - s_2]/\tau_{f2}, & V_M < V_{Th(M)}. \end{cases}
\end{aligned}$$

The set of points satisfying $f(V_L, V_I, s) = 0$ and $g(V_I, V_L, s_{AB \rightarrow I}) = 0$ are called the V_L and V_I nullclines, respectively. In slow time, (9) and (10) imply that any trajectory is forced to lie on the V_L and V_I nullclines while s_1 slowly evolves and s_2 instantaneously jumps between s_{2min} and 1 whenever V_M crosses the threshold $V_{Th(M)}$. In slow time, $s_{AB \rightarrow M}$ jumps to 1 whenever V_{AB} increases above $V_{Th(AB)}$ and decays exponentially to 0 whenever V_{AB} decreases below $V_{Th(AB)}$. Note that this slow decay of $s_{AB \rightarrow M}$ implies from (11) that the voltage V_M slowly increases from V_M^* toward $E_{leak, M}$. We choose $V_{Th(M)}$ to lie between these two values such that the time for V_M to increase from V_M^* to $V_{Th(M)}$ equals a predetermined time called T_C .

Note that when $\bar{g}_{AB \rightarrow M} = 0$, then V_M is always greater than $V_{Th(M)}$, and we refer to *MCN1* as being tonically active. In this case, $s_2 = 1$. Alternatively, when $\bar{g}_{AB \rightarrow M}$ is sufficiently large, then V_M goes above and below $V_{Th(M)}$ in pyloric time and we say that *MCN1* is rhythmically active. In this case, s_2 jumps between s_{2min} and 1 each time V_M crosses $V_{Th(M)}$. By choosing τ_{r1} and τ_{f1} small relative to P_{AB} , we note that V_M may cross $V_{Th(M)}$ several times before V_L crosses V_T .

To define fast equations, let $\zeta = t/\epsilon$ in (1)–(3), (5), and (7)–(8); then set $\epsilon = 0$ to obtain

$$\begin{aligned}
(16) \quad & \frac{dV_L}{d\zeta} = f(V_L, V_I, s), \\
(17) \quad & \frac{dV_I}{d\zeta} = g(V_I, V_L, s_{AB \rightarrow I}), \\
(18) \quad & \frac{dV_M}{d\zeta} = -g_{leak, M}[V_M - E_{leak, M}] - \bar{g}_{AB \rightarrow M} s_{AB \rightarrow M}(t)[V_M - E_{AB \rightarrow M}], \\
(19) \quad & \frac{ds_{AB \rightarrow M}}{d\zeta} = \begin{cases} [1 - s_{AB \rightarrow M}]/\tau_M, & V_{AB} \geq V_{Th(AB)}, \\ 0, & V_{AB} < V_{Th(AB)}, \end{cases}
\end{aligned}$$

$$(20) \quad \frac{ds_2}{d\zeta} = \begin{cases} [1 - s_2]/\tau_{r2}, & V_M \geq V_{Th(M)}, \\ [s_{2min} - s_2]/\tau_{f2}, & V_M < V_{Th(M)}, \end{cases}$$

$$(21) \quad \frac{ds_1}{d\zeta} = 0.$$

Therefore, in fast time V_L and V_I evolve according to the dynamics of $f(V_L, V_I, s)$ and $g(V_I, V_L, s_{AB \rightarrow I})$, and s_2 increases and decreases between 1 and s_{2min} while s_1 remains constant. These equations govern transitions between the different branches of the V_I and V_L nullclines. These transitions occur instantaneously with respect to the slow flow.

2.2. Geometry of nullclines. In the previous subsection, we derived reduced fast and slow equations which govern the flow of trajectories in relevant phase spaces. For the slow equations (9)–(15), the slow variable s_1 evolves according to (14), while the activity of the fast variables V_L , V_I , V_M , and s_2 is constrained through the algebraic equations (9), (10), (11), and (15). Note that $s_{AB \rightarrow M}$ is a fast variable whenever $V_{AB} \geq V_{Th(AB)}$ according to (13) and is a slow variable whenever $V_{AB} < V_{Th(AB)}$ according to (12). For the fast equations (16)–(21), the slow variables act as parameters. Fixed points of the fast equations correspond to situations where the V_I and V_L nullclines intersect. We will be interested in situations where the existence and stability of fixed points of the fast subsystem change. Generally speaking, this may occur because the slow variable s_1 causes the fast system to undergo a saddle-node bifurcation, or if s_{AB} changes, causing the position of the nullclines to change on the fast timescale in phase space. Below, we show geometrically how these situations may arise.

We shall first consider the case when the synapse from *MCN1* to *LG* is not voltage dependent. We do this by letting $s_\infty(V_L) \equiv 1$. The effect of the voltage dependency of this synapse is considered in section 5. We find the explicit equations for the nullclines by solving (9) for V_L and (10) for V_I to find that

$$(22) \quad V_L = F(V_I, s) = \frac{g_{leak,L} E_{leak,L} + \bar{g}_{I \rightarrow L} n_\infty(V_I) E_{I \rightarrow L} + \bar{g}_s(V_L) s E_{exc}}{g_{leak,L} + \bar{g}_{I \rightarrow L} n_\infty(V_I) + \bar{g}_s(V_L) s}$$

and

$$(23) \quad V_I = G(V_L, s_{AB \rightarrow I}) = \frac{g_{leak,I} E_{leak,I} + \bar{g}_{L \rightarrow I} n_\infty(V_L) E_{L \rightarrow I} + \bar{g}_{AB \rightarrow I} s_{AB \rightarrow I}(t) E_{AB \rightarrow I}}{g_{leak,I} + \bar{g}_{L \rightarrow I} n_\infty(V_L) + \bar{g}_{AB \rightarrow I} s_{AB \rightarrow I}(t)}.$$

A simultaneous solution to (9) and (10) can be found graphically by plotting $F(V_I, s)$ versus $G(V_L, s_{AB \rightarrow I})$. An intersection of these two nullclines corresponds to a fixed point of the fast equations. However, the position of the nullclines in $V_I - V_L$ phase space changes as a function of s and s_{AB} ; see Figure 3. In general, increases (decreases) in s move the V_L nullcline to the right (left), either in slow time due to changes in s_1 or in fast time due to changes in s_2 . The V_I nullcline has two possible positions in phase space depending on whether $s_{AB \rightarrow I} = 0$ or 1. The nullcline corresponding to $s_{AB \rightarrow I} = 1$ is lower in phase space than the one corresponding to $s_{AB \rightarrow I} = 0$. We note that the left branch of the V_I nullcline shifts down much more than the right branch since on the right branch V_I is already close to $E_{AB \rightarrow I}$ independent of $s_{AB \rightarrow I}(t)$. The number and stability of fixed points also changes as a function of s and $s_{AB \rightarrow I}$. We identify four important values of $(s, s_{AB \rightarrow I})$ as $(s_L^{off}, 0)$, $(s_L^{on}, 1)$,

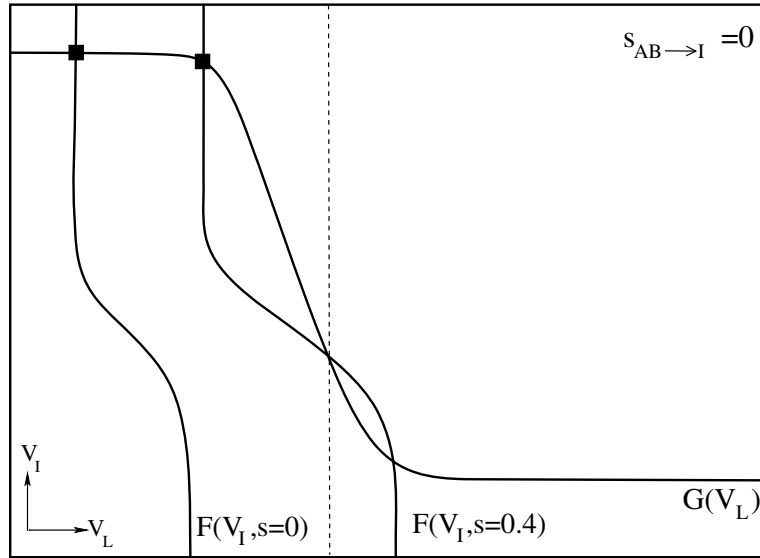


Figure 3. The V_L and V_I nullclines plotted in phase space for two different values of $s(t)$. The V_L nullcline is labeled F , the V_I nullcline is labeled G , and the dashed vertical line is $V_L = V_T$. When $s = 0$, the V_L nullcline is to the far left. As s increases, the V_L nullcline shifts to the right. Solid squares denote fixed points of the fast equations (16)–(21).

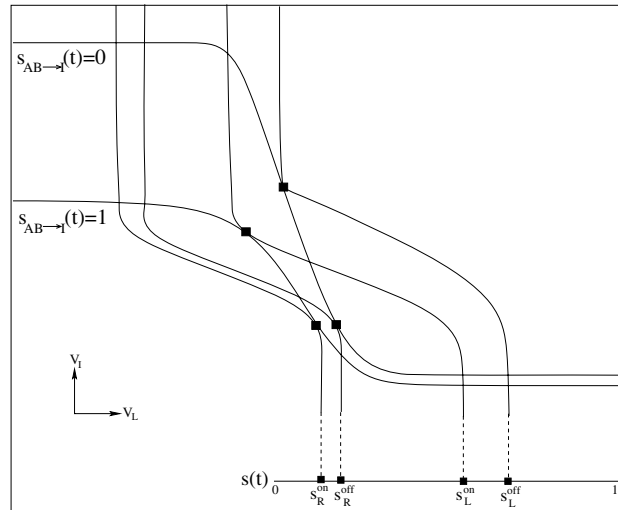


Figure 4. Position of the V_L and V_I nullclines for $(s, s_{AB \rightarrow I}) = (s_R^{on}, 1)$, $(s_R^{off}, 0)$, $(s_L^{on}, 1)$, and $(s_L^{off}, 0)$. At these four points, the nullclines intersect tangentially, resulting in the loss (or gain) of two fixed points through a saddle-node bifurcation.

$(s_R^{off}, 0)$, and $(s_R^{on}, 1)$; see Figure 4. The superscripts *off* and *on* refer to the AB input to $Int1$ which can be either absent (*off*) or present (*on*). These points correspond to values when the two nullclines intersect tangentially resulting in the loss (or gain) of two fixed points through a saddle-node bifurcation. Because s_1 is increasing on the left branches and decreasing on

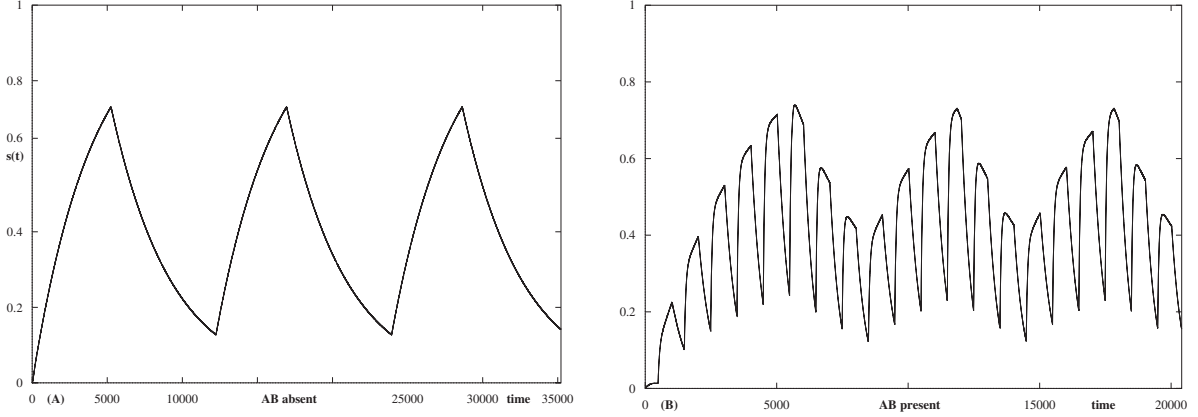


Figure 5. (A) s versus t for the case when the MCN1 to LG excitation is constant ($s_2 = 1$). s increases to 1 with rate $1/\tau_{r1}$ when $V_L \leq V_T$ and s decreases to 0 with rate $1/\tau_{f1}$ when $V_L > V_T$. (B) s versus t for the case when the MCN1 to LG excitation is rhythmic. When $V_L \leq V_T$, s_1 increases to 1 with rate $1/\tau_{r1}$ and s_2 jumps between 1 and s_{2min} when $s_{AB \rightarrow M}(t)$ jumps between 0 and 1. When $V_L > V_T$, s_1 decreases to 0 with rate $1/\tau_{f1}$ and s_2 jumps between 1 and s_{2min} when $s_{AB \rightarrow M}(t)$ jumps between 0 and 1.

the right, the ordering of these bifurcation points is $s_R^{on} < s_R^{off} < s_L^{on} < s_L^{off}$. These values can be calculated analytically; see the appendix. For our numerical simulations, we chose the parameters such that $s_R^{on} = .11$, $s_R^{off} = .127$, $s_L^{on} = .31$, and $s_L^{off} = .73$.

On the slow timescale, the solution trajectory must lie at the intersection of the V_I and V_L nullclines, i.e., at a fixed point of the fast subsystem. Thus to understand the evolution of trajectories in the $V_I - V_L$ phase space, we need to understand how the position of fixed points changes as a function of s and s_{AB} .

Let us first consider the case when $s_{AB \rightarrow M}(t) \equiv 0$. Then MCN1 is tonically active and sits at a value of $E_{leak,M}$. $E_{leak,M}$ is chosen to be larger than $V_{Th(M)}$ which, as we see from (15), allows $s_2 = 1$. As a result, we have $s(t) = s_1(t) * 1$ which means that $s(t)$ increases toward 1 with time constant τ_{r1} when $V_L < V_T$ and decreases toward 0 with time constant τ_{f1} when $V_L > V_T$ (see Figure 5(A)).

From (22), as s slowly increases, the V_L nullcline slowly shifts to the right, thus causing the position of the stable fixed point to shift to the right. This continues until the V_L nullcline shifts far enough to the right so that the stable fixed point on the left branches of the nullclines is lost through a saddle-node bifurcation when $s = s_L^{off}$; see Figure 6. Once the fixed point is lost, the trajectory is forced to jump on the fast timescale (see (16)–(17)) to the only remaining stable fixed point which is on the right branches of the nullclines. This jump pushes V_L above V_T causing $s(t)$ to begin to decrease. When s decreases, the V_L nullcline slowly shifts to the left until the stable fixed point on the right branches of the V_L and V_I nullclines similarly undergoes a saddle-node bifurcation at $s = s_R^{off}$. The trajectory then makes a jump back to the left branches of the nullclines which forces V_L below V_T . Similar dynamics occur when $s_{AB \rightarrow I}(t) \equiv 1$, except now the trajectory would pass through the bifurcation points s_L^{on} and s_R^{on} during its transition between left and right branches.

When the MCN1 excitation to LG is rhythmic instead of tonic, s_2 changes on the fast timescale between 1 and s_{2min} as V_M crosses over $V_{Th(M)}$ while s_1 increases toward 1 when

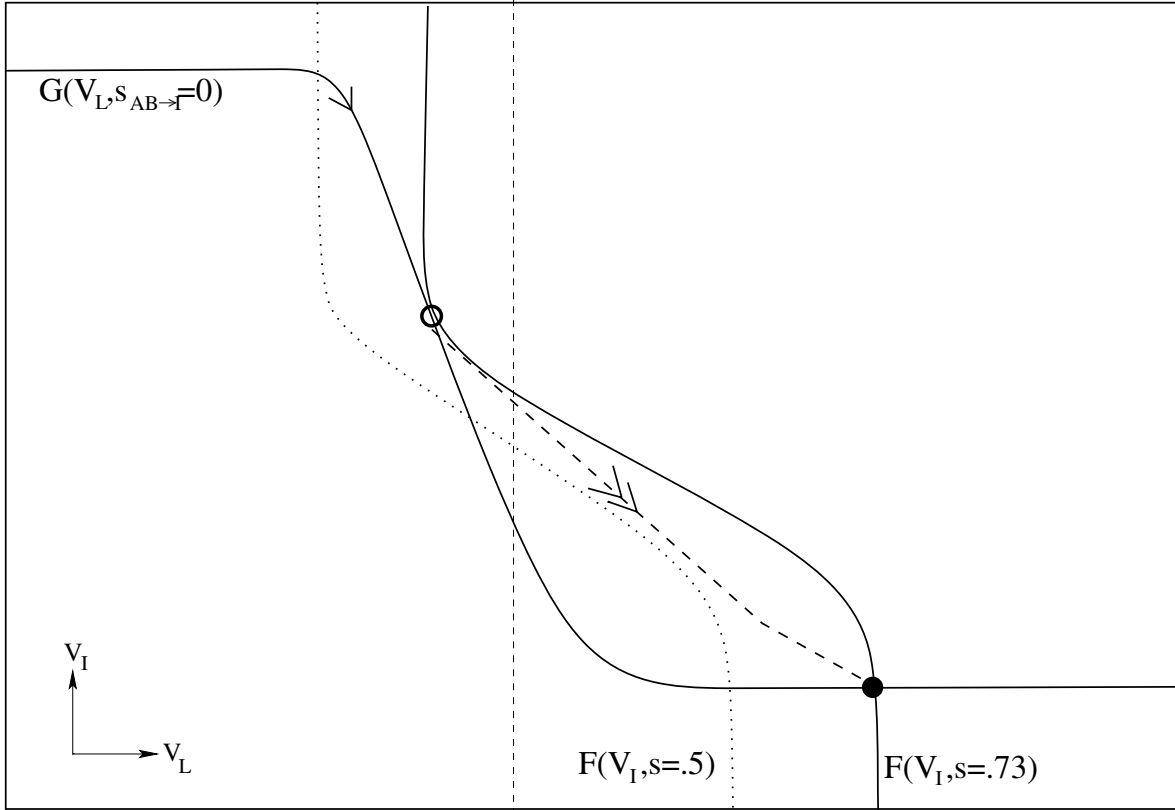


Figure 6. V_L and V_I nullclines for different values of s when $s_{AB \rightarrow I}(t) = 0$. The dashed vertical line is $V_L = V_T$. When $s = 0.5$, the fixed point is on the left branches of the V_L and V_I nullclines (V_L nullcline dotted). When $s = s_L^{off}$, the fixed point undergoes a saddle-node bifurcation at \circ . The trajectory is therefore forced to jump (dashed line with double arrows) to the stable fixed point (shown by \bullet) on the right branches of the nullclines where $V_L > V_T$.

$V_L \leq V_T$ and decreases toward 0 when $V_L > V_T$ on the slow timescale. This causes $s(t)$ to generally have a shape as shown in Figure 5(B). Notice that the envelope of $s(t)$ activity is the same as in the tonic excitability case seen in Figure 5(A), but now there are rapid changes in $s(t)$ due to the rapid changes in $s_2(t)$. The jump of s_2 between s_{2min} and 1 causes the V_L nullcline to instantaneously jump to the right when s_2 jumps to 1 and instantaneously jump to the left when s_2 jumps to s_{2min} . The distance of these jumps in the V_L nullcline, calculated from (22), is $F(V_I, s_1 * 1) - F(V_I, s_1 * s_{2min})$. Note that in the MCN1 rhythmic case, fixed points can be lost in two different ways. They may be lost as before through a saddle-node bifurcation as s is slowly changing due to changes in s_1 ; see Figure 7(A). Or they may be lost when s_2 changes on the fast timescale. For example, on the left branches, it may be that $s_1 * s_{2min} < s_L^{off}$, but $s_1 * 1 > s_L^{off}$. In this case, the fixed point would be lost if s_{2min} changed to 1 due to a change in MCN1 activity; see Figure 7(B). On the right branches, it may be that $s_1 * 1 > s_R^{off}$, but $s_1 * s_{2min} < s_R^{off}$. In this case, the fixed point would be lost when s_2 changes from 1 to s_{2min} .

In the case where $s_{AB \rightarrow I}(t)$ is a square wave, the trajectory will always lie on a nullcline

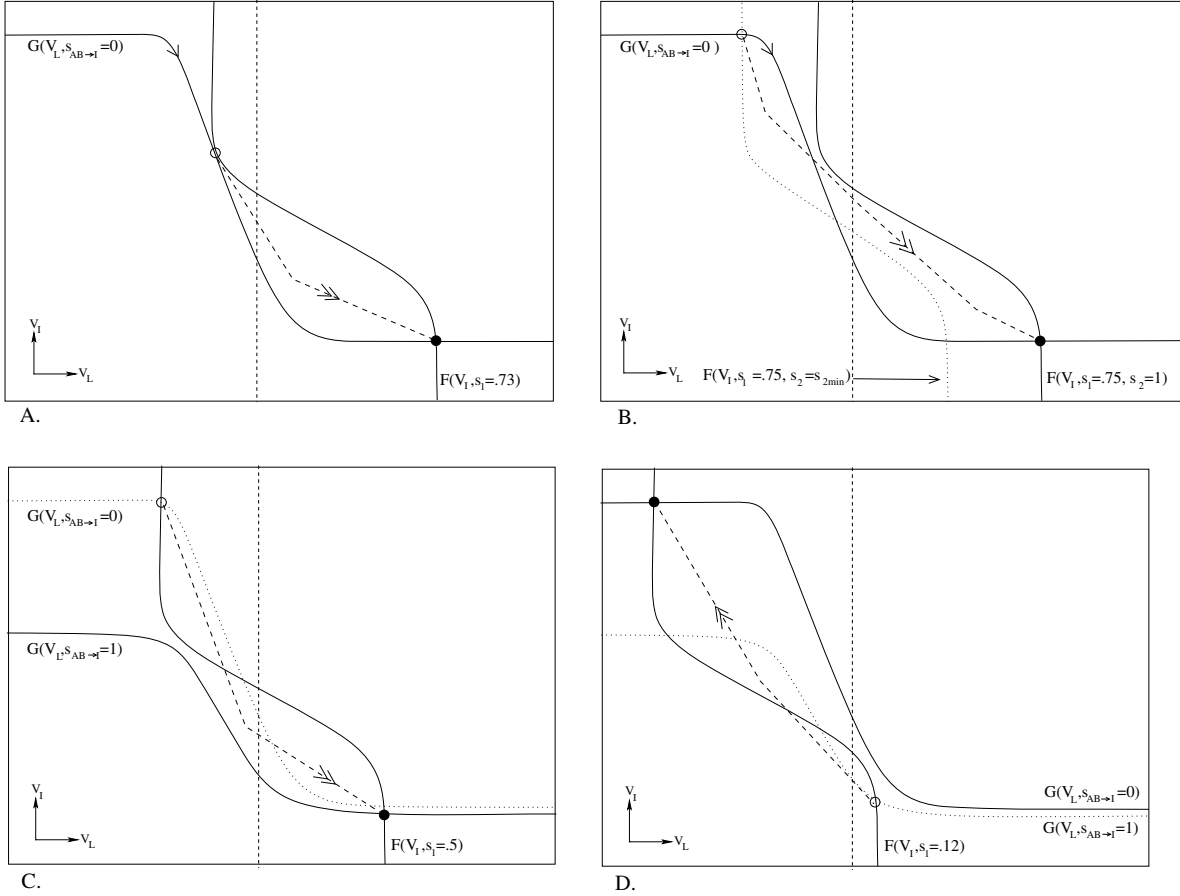


Figure 7. For MCN1 rhythmic, fixed points can be lost in two ways: through a saddle-node bifurcation as s slowly changes due to s_1 or when s_2 changes on the fast timescale. In all figures, the dashed vertical line is $V_L = V_T$. (A) On the left branches of the nullclines, $s_2 = 1$ and s_1 moves the V_L nullcline to the right resulting in a saddle-node bifurcation of the fixed point at \circ once $s = s_L^{off}$. The trajectory is forced to jump to the stable fixed point on the right branches of the nullclines (shown by \bullet). A similar transition can also occur when $s_{AB \rightarrow I} = 1$ and s_1 reaches s_L^{on} . (B) When s_2 jumps from s_{2min} to 1, the V_L nullcline jumps from the left (dotted nullcline) to the right (solid nullcline). Thus the fixed point on the left branches of the nullclines is instantaneously lost because $s > s_L^{off}$ and the trajectory will jump to the fixed point on the right branches of the nullclines (shown by \bullet). A similar transition can also occur when $s_{AB \rightarrow I} = 1$ and s_2 jumps to 1 such that $s > s_L^{on}$. (C) When MCN1 is rhythmic and $s_{AB \rightarrow I}(t)$ oscillates between 0 and 1, the fixed point can be lost in another way. While $s_2 = 1$ and $s_{AB \rightarrow I}(t)$ jumps from 0 to 1 (the position of the V_I nullcline jumps from the upward dotted nullcline to the lower solid nullcline), the fixed point on the left branches of the nullclines (shown by \circ) is instantaneously lost because $s > s_L^{on}$ and the solution trajectory is forced to jump to the fixed point on the right branches of the nullclines (shown by \bullet). (D) On the right branches of the nullclines for MCN1 tonic, when $s_{AB \rightarrow I}$ jumps from 1 to 0 (the position of the V_I nullcline jumps from the lower dotted nullcline to the upward solid nullcline), the fixed point (shown by \circ) is instantaneously lost because $s_R^{on} < s < s_R^{off}$ and the solution trajectory must jump to the stable fixed point on the left branches of the nullclines (shown by \bullet).

with either $s_{AB \rightarrow I} = 0$ or $s_{AB \rightarrow I} = 1$. Now fixed points can be lost in three different ways. Consider the left branches. As before, a fixed point can be lost as s increases slowly through a bifurcation point or instantaneously as s_2 changes from s_{2min} to 1. The third way it can be

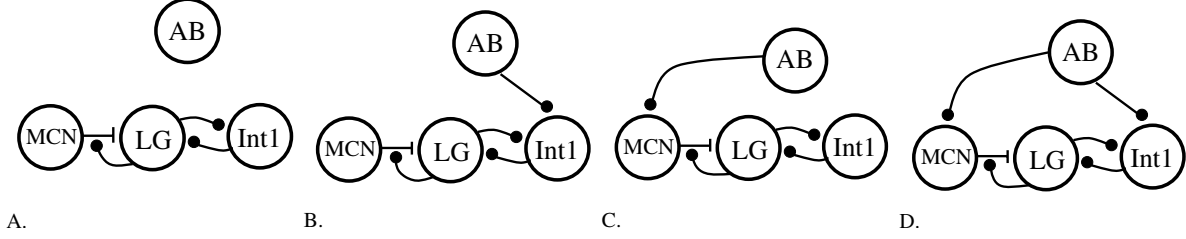


Figure 8. Circuitry for cases 1–4. (A) The AB inputs to $MCN1$ and to $Int1$ are absent. (B) The AB input to $Int1$ is present but the AB input to $MCN1$ is absent. (C) The AB input to $MCN1$ is present but the AB input to $Int1$ is absent. (D) The AB inputs to $Int1$ and to $MCN1$ are present.

lost is if $s_L^{off} > s > s_L^{on}$ and $s_{AB \rightarrow I}$ switches from 0 to 1; see Figure 7(C) (see Figure 7(D) for the analogous loss of a fixed point on the right branches).

3. Different cases for the gastric mill frequency. To understand how the two different inputs of AB and $MCN1$ modulate the gastric mill frequency, we parallel the study of Wood et al. [30] by considering four different cases (see Figure 8):

Case 1. Tonic $MCN1$ excitation with the AB input to $Int1$ absent.

Case 2. Tonic $MCN1$ excitation with the AB input to $Int1$ present.

Case 3. Rhythmic $MCN1$ excitation with the AB input to $Int1$ absent.

Case 4. Rhythmic $MCN1$ excitation with the AB input to $Int1$ present.

In each case, we shall prove the existence, local uniqueness, and stability of a periodic solution and then calculate the period of this solution. The proofs of existence, local uniqueness, and stability of periodic solutions exploit the different timescales. In Cases 2 through 4, this will reduce to finding fixed points of appropriate one-dimensional maps. The proofs construct singular periodic solutions which are valid at $\epsilon = 0$, whose existence, local uniqueness, and stability can be extended to the ϵ sufficiently small case [20].

In the biological circuit it is known that the synapse from $MCN1$ to LG is dependent on the voltage of LG . For mathematical clarity, we shall postpone discussing the voltage dependent case until section 5. Instead, we shall first concentrate on the voltage independent case where we set $s_\infty(V_L) \equiv 1$.

Case 1: Tonic $MCN1$ excitation with the AB input to $Int1$ absent. When considering Case 1, we set $\bar{g}_{AB \rightarrow I} = 0$ and $\bar{g}_{AB \rightarrow M} = 0$ in (2) and (3) so that all input from AB is absent. When $\bar{g}_{AB \rightarrow M} = 0$, $V_M > V_{Th(M)}$ for all t and $MCN1$ is tonically active. This allows us to set $s_2 \equiv 1$ so that $s = s_1 * s_2$ will only follow the dynamics of s_1 .

In Case 1, the only way a fast transition between branches can occur is by s_1 passing through the bifurcation points s_L^{off} or s_R^{off} . To construct a periodic solution, let $s_1(0) = s_R^{off}$ such that the trajectory at $t = 0^-$ is at the bifurcation point on the right branches at the intersection of the V_I and V_L nullclines; see Figure 9. At $t = 0^+$, the trajectory jumps back to the left branches at the intersection of the nullclines; see Figure 9(A). On these branches, $V_L < V_T$ and thus s_1 will increase until it reaches the bifurcation point s_L^{off} at $t = T_1$; see Figure 9(B)–(C). The trajectory will jump back to the right branch and since $V_L > V_T$, s_1 will now decrease until it comes back to s_R^{off} at $t = T_2$; see Figure 9(D). Thus the value of s_1 will have returned to its original value at time T_2 . Since all the fast variables are slaved

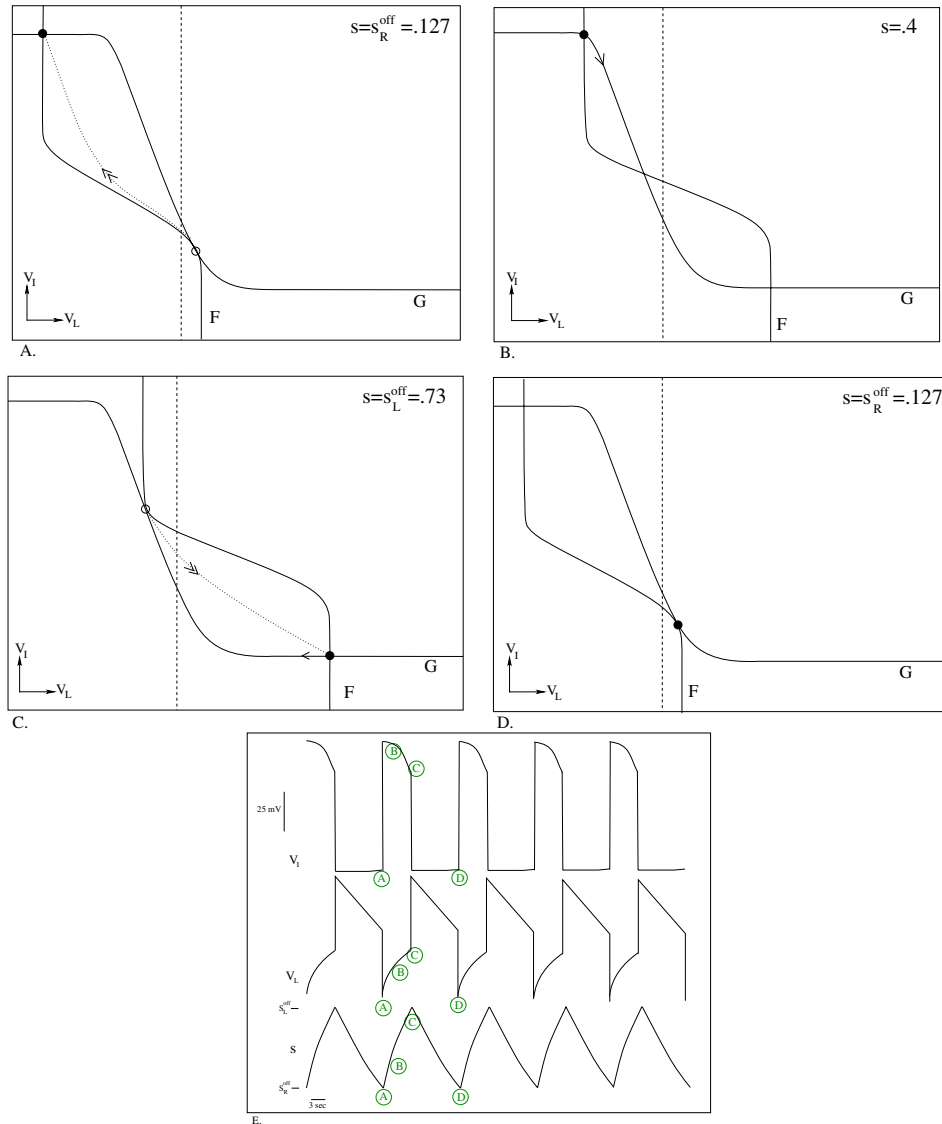


Figure 9. Plots of the V_I and V_L nullclines for different values of s in Case 1. \bullet marks the position of the trajectory when it is at a stable fixed point, \circ marks the point from which the trajectory will jump when the stable fixed point bifurcates, and the dotted lines indicate the position of the trajectory during the jumps. The arrows show the direction of flow. The dashed vertical line marks the threshold, V_T . In (A), $s = s_R^{\text{off}}$, which is the point at which the saddle-node bifurcation occurs on the right branches of the nullclines. Thus, the trajectory will be forced to lie on the stable fixed point on the left branches of the nullclines. (B) On the left branches of the nullclines, $V_L < V_T$, which means that s will begin to increase toward 1. (C) s continues to increase until it reaches the value s_L^{off} , where the stable fixed point on the left branches of the nullclines undergoes a saddle-node bifurcation. The trajectory is, therefore, forced to jump to the fixed point on the right branches of the nullclines. This jump causes s to cross above V_T so that s begins to decrease. (D) s has decreased to $s = s_R^{\text{off}}$, at which time the fixed point on the right branches is again lost through a saddle-node bifurcation and the trajectory is forced to return to the upper left branches of the nullclines. Therefore, the solution trajectory lies on a periodic orbit. (E) The voltage traces of LG and Int1 are plotted as s increases and decreases between s_L^{off} and s_R^{off} . The labels A, B, C, and D indicate where the trajectory is in the phase plane at the given values of $s(t)$, V_I , and V_L .

through (9) and (10) to the behavior of s_1 , we do not explicitly need to check their evolution during the time interval $[0, T_2]$. In this sense, proving the existence of this periodic solution has been reduced to proving that the single variable s_1 is periodic. Thus it is seen that there exists a singular periodic solution whose period is T_2 . In section 4, we will both analytically and numerically calculate T_2 .

The solution is unique and stable since if $s_1(0) > s_R^{off}$ and the trajectory was on the right branches of the nullclines, for example, then the solution can be flowed forward at time \hat{t} such that $s_1(\hat{t}) = s_R^{off}$. From here the solution trajectory would follow the dynamics described above and return to s_R^{off} at time $t = T_2 + \hat{t}$. Thus, by flowing backward in time, it is seen that $s_1(T_2) = s_1(0)$.

Case 2: Tonic MCN1 excitation with the AB input to Int1 present. In Case 2, $\bar{g}_{AB \rightarrow M} = 0$ so that $s_2 \equiv 1$ and thus the MCN1 to LG excitation is tonic. Now the AB to Int1 inhibition is present ($\bar{g}_{AB \rightarrow I} > 0$). Without loss of generality, let $m = 0$ in (2). Hence, s causes the V_L nullcline to slowly shift to the right and left as in Case 1 and $s_{AB \rightarrow I}(t)$ causes the V_I nullcline to instantaneously jump down when $s_{AB \rightarrow I}(t)$ goes to 1 and to jump back up when $s_{AB \rightarrow I}(t)$ returns to 0.

To understand the control of frequency in Case 2, we again consider the nullclines in the phase plane. When $V_L > V_T$, the V_L nullcline moves to the left slowly because τ_{f1} is large. The AB input to Int1, on the other hand, is fast and periodic so that the V_I nullcline shifts up and down repeatedly and instantaneously compared with the shift of the V_L nullcline. Thus, on the right branches of the nullclines, three cases arise for the loss of the fixed point. The first possibility is that while $s_R^{on} < s < s_R^{off}$, $s_{AB \rightarrow I}(t)$ switches from 1 to 0, forcing the V_I nullcline to jump up causing the stable fixed point to be immediately lost. This forces the trajectory to jump directly to the stable fixed point on the left branches of the V_I and V_L nullclines; see Figure 7(D).

The second possibility is that when $s_{AB \rightarrow I}(t) = 1$, s decreases until the fixed point is lost through the saddle-node bifurcation at $s = s_R^{on}$. The third possible way for the fixed point on the right branches to be lost is as in Case 1. That is, while $s_{AB \rightarrow I} = 0$, s decreases to s_R^{off} ; see Figure 9(D). Which of these cases occurs depends upon the amount of time that $s_{AB \rightarrow I}(t)$ spends in its active and inactive phases and the timing of the AB input to Int1. In other words, the timing of the periodic jumps in $s_{AB \rightarrow I}$ affects the timing of the shifts in the V_I nullcline, which in turn determines which case occurs. The fixed point on the left branch can be lost similarly to the ways discussed above. Let us say that a periodic solution obeys property A if the associated trajectory jumps from the right to left branches when $s_{AB \rightarrow I}(t)$ switches from 1 to 0 and from left to right branches through the bifurcation point s_L^{on} ; see Figure 10.

Recall that the pyloric period is much smaller than the gastric mill period. Thus, while LG is inactive ($V_L < V_T$), s_{AB} can oscillate several times, say, j times, between 0 and 1. The exact number of times depends on the time constant τ_{r1} . Similarly when LG is active ($V_L > V_T$), the number of oscillations, k , of s_{AB} depends on the time constant τ_{f1} . This implies that the periodic solution in case 2 depends on the relationship between τ_{r1} , τ_{f1} and the pyloric input frequency of AB. In the following theorem we will derive a relationship which τ_{r1} and τ_{f1} need to satisfy in order to find a periodic solution with property A. This

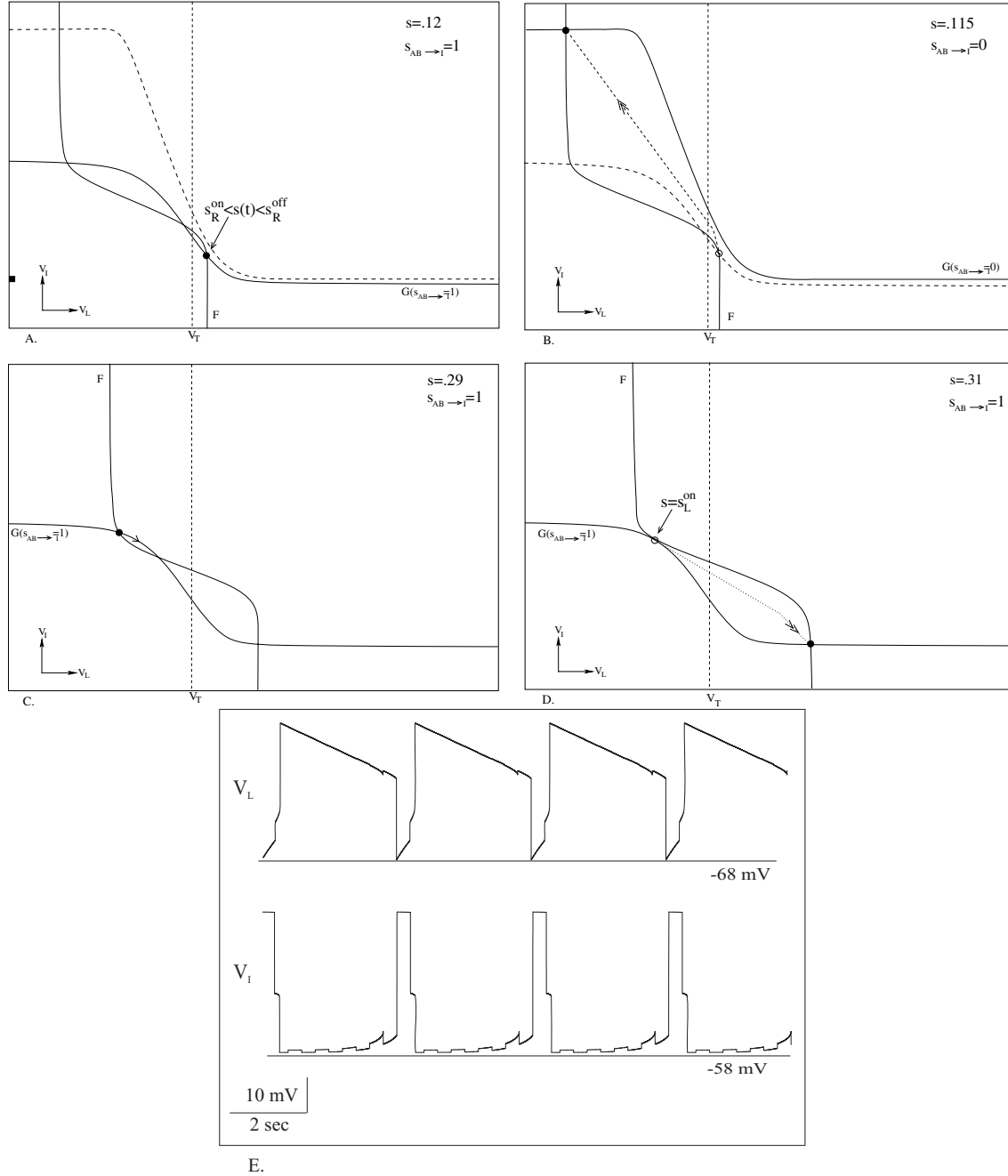


Figure 10. In Case 2, a periodic orbit obeying property A jumps from the left to right branches and from the right to left branches of the nullclines in the following way. (A) When s_1 lies between s_R^{off} and s_R^{on} , the stable fixed point lies on the right branches of the nullclines when $s_{AB \rightarrow I} = 1$. (B) As soon as $s_{AB \rightarrow I}$ jumps back to 0, the fixed point on the right branches of the nullclines is instantaneously lost because $s_1 < s_R^{off}$ and the trajectory jumps back to the left branches. (C) The trajectory lies at the stable fixed point (●) on the left branches of the nullclines where $s_{AB \rightarrow I} = 1$ and s_1 increases toward 1. (D) While $s_{AB \rightarrow I}$ remains equal to 1, s_1 increases and becomes sufficiently large for a saddle-node bifurcation to occur through s_L^{on} . (E) Voltage traces of V_L and V_I for a periodic orbit obeying property A.

involves fixing the integers j and k first. To that end define

$$(24) \quad h(k) = \frac{D_c}{\ln\left(\frac{1-s_R^{off}(s_R^{off}/s_L^{on})^{D_c/k}}{1-s_R^{off}}\right)} \ln\left(\frac{1-s_R^{off}}{1-s_L^{on}}\right) + D_c - 1.$$

Theorem. *Let k and j be integers which satisfy $j < h(k)$. There exist values $\tau_{r1}(j)$, $\tau_{f1}(k)$, and $\bar{g}_{AB \rightarrow I}$ large enough such that (1)–(3) and (7)–(8) possess a locally unique, asymptotically stable periodic solution obeying property A with period $P = (j + k + 1)P_{AB}$, where j is the number of times s_{AB} oscillates between 0 and 1, while $V_L < V_T$ and k is the number of time s_{AB} oscillates between 0 and 1 when $V_L > V_T$.*

Proof. We shall construct a Poincaré map \mathcal{P} of a certain interval \mathcal{I} into itself. Existence and stability of the periodic solution are determined by showing that \mathcal{P} is a contraction on \mathcal{I} , thereby also yielding local uniqueness of the periodic solution. To construct the periodic solution in question we will show that the associated trajectory will jump from the left to the right branches from the bifurcation point s_L^{on} . It will jump from the right to the left branches from a point $s^* \in \mathcal{I}$ at one of the times when $s_{AB \rightarrow I}$ switches from one to zero.

To construct \mathcal{I} , consider the points s_R^{off} and s_R^{on} corresponding to the bifurcation points along the right branches of the V_I - V_L nullclines when $s_{AB \rightarrow I} = 0$ (AB off) and $s_{AB \rightarrow I} = 1$ (AB on), respectively. By choosing $\bar{g}_{AB \rightarrow I}$ and τ_{f1} sufficiently large, we can guarantee that the time distance from s_R^{off} to s_R^{on} under the dynamics $s' = -s/\tau_{f1}$ is larger than $D_c P_{AB}$. Indeed the time Δt between these two points on the right branches is $\tau_{f1} \ln(s_R^{off}/s_R^{on})$, where s_R^{on} is a decreasing function of $\bar{g}_{AB \rightarrow I}$. Moreover, there exists \hat{s} such that $\hat{s} = s_R^{off} \exp(-D_c P_{AB}/\tau_{f1})$. Thus the time distance from s_R^{off} to \hat{s} on the right branches is exactly $D_c P_{AB}$. We let $\mathcal{I} = [\hat{s}, s_R^{off}]$; see Figure 11. Note that at this point, we are only stating that we need τ_{f1} sufficiently large. Below, we will be more specific.

We next show that \mathcal{I} maps into itself under the flow if τ_{r1} and τ_{f1} are chosen appropriately. We flow the endpoints of the interval \mathcal{I} , s_R^{off} , and \hat{s} , through one cycle of the V_I and V_L oscillation and show that these endpoints are mapped into \mathcal{I} . Thus by continuous dependence on initial conditions, all points in \mathcal{I} will map into \mathcal{I} .

First consider a trajectory $s_a(t)$ where $s_a(0) = s_R^{off}$ and the trajectory is on the right branch. Next let $s_{AB \rightarrow I}(0^-) = 1$ and $s_{AB \rightarrow I}(0^+) = 0$, so that the trajectory jumps back to the left branch at $t = 0^+$. The dynamics of s_a on the left branches obey $s' = (1-s)/\tau_{r1}$. By choosing

$$(25) \quad \tau_{r1}(j) = (j + 1 - D_c)P_{AB} / \ln([1 - s_R^{off}]/[1 - s_L^{on}]),$$

we can guarantee that $s_a([j + 1 - D_c]P_{AB}) = s_L^{on}$. This means that the trajectory which starts at s_R^{off} will leave the left branches of the nullclines through the bifurcation point s_L^{on} along the $s_{AB \rightarrow I} = 1$ nullcline at time $t = (j + 1 - D_c)P_{AB}$.

Next consider a trajectory $s_b(t)$ with the initial condition given by $s_b(0) = \hat{s}$. Recall that the time distance from s_R^{off} to \hat{s} on the right branches is given by $\tau_{f1} \ln(s_R^{off}/\hat{s})$. On the left branches, the time between these points is governed by τ_{r1} and is equal to $\tau_{r1} \ln([1 - \hat{s}]/[1 -$

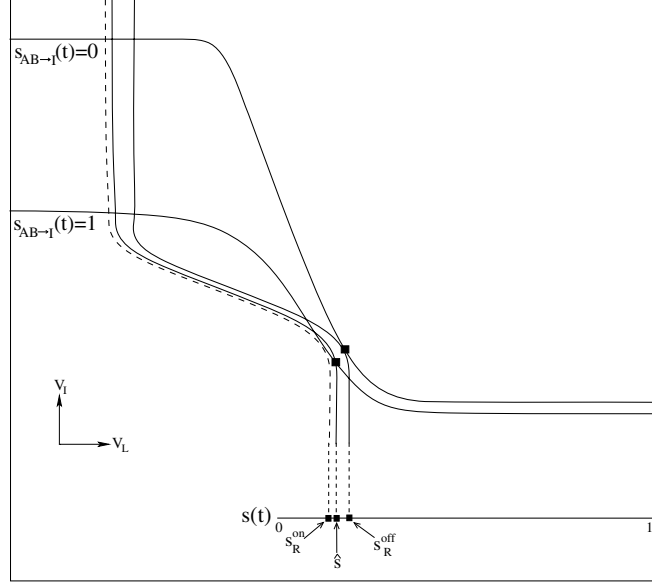


Figure 11. To define the Poincaré map for Case 2, let $I = [\hat{s}, s_R^{off}]$, where $\hat{s} = s_R^{off} \exp(-D_c P_{AB}/\tau_{f1})$. Note that τ_{f1} is chosen sufficiently large to ensure that $\hat{s} > s_R^{on}$.

s_R^{off}). Thus if

$$(26) \quad \tau_{r1} < \tau_{f1} \frac{\ln(s_R^{off}/\hat{s})}{\ln([1-\hat{s}]/[1-s_R^{off}])},$$

then the time between these points on the left branches will be less than that on the right branches and, in particular, will be less than $D_c P_{AB}$. This type of time compression between cells across a jump is analogous to fast threshold modulation [26]. Thus the trajectory starting with initial condition at \hat{s} at $t = 0$ will reach s_L^{on} when $s_{AB \to I} = 1$ at a time T_1 bounded between $(j+1-D_c)P_{AB}$ and $(j+1)P_{AB}$. Therefore, any trajectory with $s(0) \in \mathcal{I}$ will do the same. We also note that once trajectories with initial conditions $s_a(0)$ and $s_b(0)$ jump from the right branches of the nullclines to the left branches, the interval \mathcal{I} becomes inverted so that the trajectory with initial condition $s_a(0)$ becomes the leading cell.

Note that the time between any two trajectories remains invariant while they both evolve on the left branches and even across the jump back to the right branches. That the trajectories remain the same time distance apart on the left branches follows from the fact that they both obey the same differential equation ($s' = (1-s)/\tau_{r1}$). Moreover, since they leave the left branches through the same point s_L^{on} , the time distance between them when the leading cell reaches the bifurcation point is the same as the time distance apart when the trailing cell reaches this point. When both trajectories are on the right branches, the time distance again remains invariant since both trajectories evolve under $s' = -s/\tau_{f1}$. In particular, the time distance between $s_a(T_1)$ and $s_b(T_1)$ is less than $D_c P_{AB}$.

Consider again the trajectory $s_a(t)$ which had $s_a(0) = s_R^{off}$ and $s_a([j+1-D_c]P_{AB}) = s_L^{on}$. We want this trajectory to spend k oscillations of s_{AB} on the right branches. We also want

the trajectory to be in a position to jump back to the left branches when $s_{AB \rightarrow I}$ switches from one to zero. Finally, since we want \mathcal{I} to map into itself, we choose

$$(27) \quad \tau_{f1}(k) = \frac{(k + D_c)P_{AB}}{\ln(s_L^{on}/\hat{s})},$$

such that $s_a([j + k + 1]P_{AB}) = \hat{s}$. Note that by substituting $\hat{s} = s_R^{off} \exp(-D_c P_{AB}/\tau_{f1})$ into (27) and solving for τ_{f1} , we obtain

$$(28) \quad \tau_{f1}(k) = \frac{kP_{AB}}{\ln(s_L^{on}/s_R^{off})}.$$

In other words, with the choices of τ_{r1} and τ_{f1} that we have made, the trajectory with initial condition s_R^{off} is mapped back to \hat{s} at a time $T_2^- = (j + k + 1)P_{AB}$.

Next consider the trajectory $s_b(t)$ where $s_b(0) = \hat{s}$ and $s_b(T_1) = s_L^{on}$. To construct the Poincaré map, we need $s_b(T_2^-) \in \mathcal{I}$. Thus we need $\hat{s} < s_b(T_2^-) < s_R^{off}$. That $\hat{s} < s_b(T_2^-)$ follows by continuity since $\hat{s} = s_a(T_2^-) < s_b(T_2^-)$. The value $s_b(T_2^-) < s_R^{off}$ since the time distance from s_R^{off} to $s_a(T_2^-) = \hat{s}$ is $D_c P_{AB}$, whereas the time distance from $s_b(T_2^-)$ to $s_a(T_2^-)$ is less than $D_c P_{AB}$.

We have just shown that the trajectories whose s values are associated with the endpoints of the interval \mathcal{I} have s values mapped back to \mathcal{I} after a time T_2^- . Thus by continuity with respect to initial conditions, any trajectory with $s(0) \in \mathcal{I}$ will end up with $s(T_2^-) \in \mathcal{I}$ at a time when $s_{AB \rightarrow I}$ will switch from one to zero. Therefore we can define a one-dimensional Poincaré map $\mathcal{P} : \mathcal{I} \rightarrow \mathcal{I}$ where $\mathcal{P}(s) = s(T_2^-)$.

To show that \mathcal{P} is a contraction mapping on \mathcal{I} let $s_a(0) > s_b(0) \in \mathcal{I}$ be arbitrary. Let Δt denote the time on the right branch between them. At $t = 0^+$, the trajectories jump back to the left branch. Because of our choice of time constants $\tau_{r1}(j)$ and $\tau_{f1}(k)$, the new time between these points is less than Δt . As before the time distance between these trajectories remains invariant as they evolve along the left branches, across the jump to the right branches, and then back to \mathcal{I} . Since this new time is less than the original time, $s_a(T_2^-) - s_b(T_2^-) < \alpha[s_a(0) - s_b(0)]$, where $\alpha < 1$ is dependent on τ_{r1} and τ_{f1} . Therefore \mathcal{P} is a contraction. As a result, there exists a unique value $s_{Case\ 2}^* \in \mathcal{I}$ such that $\mathcal{P}(s_{Case\ 2}^*) = s_{Case\ 2}^*$. This value is asymptotically stable and corresponds to a locally unique singular periodic solution of equations (9)–(21). For ϵ small, results in [20] show that an actual solution to (1)–(3) and (7)–(8) exists within an $O(\epsilon)$ neighborhood of the singular one.

Equation (26) provides a condition on the time constants τ_{f1} and τ_{r1} for which the theorem holds. This condition can be translated into a relationship between the integers j and k . Namely, by substituting $\hat{s} = s_R^{off} \exp(-D_c P_{AB}/\tau_{f1})$ into the fraction on the right-hand side of (26), we see that the numerator of that expression reduces to $D_c P_{AB}/\tau_{f1}$, while the denominator reduces to

$$(29) \quad \ln \left(\frac{1 - s_R^{off} \exp(-D_c P_{AB}/\tau_{f1})}{1 - s_R^{off}} \right).$$

Now substituting (28) into (29) and then substituting the resulting expression into (26), we obtain

$$(30) \quad \tau_{r1} < \tau_{f1} \frac{(D_c P_{AB} / \tau_{f1})}{\ln \left(\frac{1 - s_R^{off} (s_R^{off} / s_L^{on})^{D_c/k}}{1 - s_R^{off}} \right)}.$$

Canceling τ_{f1} from the right-hand side, substituting τ_{r1} from (25), and solving for j , we obtain

$$(31) \quad j < \frac{D_c}{\ln \left(\frac{1 - s_R^{off} (s_R^{off} / s_L^{on})^{D_c/k}}{1 - s_R^{off}} \right)} \ln \left(\frac{1 - s_R^{off}}{1 - s_L^{on}} \right) + D_c - 1.$$

The right-hand side of (31) is what we called $h(k)$ in the statement of the theorem.

Remark. Note that if (31) is not satisfied, then we cannot find time constants τ_{r1} and τ_{f1} for which a periodic solution satisfying property A exists. However, by choosing τ_{r1} and τ_{f1} differently, we could instead have easily constructed a periodic solution whose s_1 value passed through the bifurcation point s_R^{off} on the transition from right to left branches and which jumped back to the right branches with $s_1 \in (s_L^{on}, s_L^{off})$ when $s_{AB \rightarrow I}$ switched from one to zero.

Case 3: Rhythmic MCN1 excitation with AB input to Int1 absent. In Case 3, the input from AB to MCN1 is present ($\bar{g}_{AB \rightarrow M} > 0$) so that the MCN1-elicited excitation to LG is rhythmic. Once again, we set $\bar{g}_{AB \rightarrow I} = 0$ so that the V_I nullcline remains at a fixed position. In this case, s_2 jumps instantaneously between s_{2min} and 1, while s_1 increases with rate $1/\tau_{r1}$ and decreases with rate $1/\tau_{f1}$, thus causing the activity of s to be rhythmic.

Again, consider the nullclines. Suppose the trajectory is at the stable fixed point on the right branches of the nullclines. Thus, s_1 is decreasing and slowly pushing the V_L nullcline to the left. Recall that s_2 jumps between 1 and s_{2min} as V_M changes. The jumps in s_2 cause the V_L nullcline to shift to the right and left on the fast timescale. The size of the shift in the V_L nullcline depends on the value of s_{2min} . The trajectory eventually jumps to the fixed point on the left branches of the nullclines when (a) $s_2 = 1$ and s_1 moves the fixed point to the position where the nullclines are tangent, i.e., $s_1 = s_R^{off}$, or (b) when $s_2 = s_{2min}$ and s_1 decreases to s_R^{off} / s_{2min} moving the fixed point to the position where the nullclines are tangent, or (c) when s_2 jumps to s_{2min} resulting in an instantaneous shift of the V_L nullcline past the point of bifurcation of the fixed points. Which case occurs depends on the speed at which s_1 decreases (τ_{f1}), the amount of time the V_L nullcline spends being shifted to the left by s_2 (the amount of time that $s_{AB \rightarrow M}(t)$ spends in its active or inactive phases), and the timing of the instantaneous shifting of the V_L nullcline (timing of the AB input to MCN1).

Once the trajectory has jumped to the left branches of the nullclines, the V_L nullcline slowly shifts to the right due to s_1 and then instantaneously jumps to the left when $V_M < V_{Th(M)}$. Again, the trajectory eventually jumps to the fixed point on the right branches of the nullclines when (a') $s_2 = 1$ and s_1 moves the fixed point to the position where the nullclines are tangent (i.e., $s_1 = s_L^{off}$; see Figure 7(A)), or when (b') $s_2 = s_{2min}$ and s_1 moves the fixed point to the position where the nullclines are tangent, or when (c') s_2 jumps to 1 resulting in an

instantaneous shift of the V_L nullcline past the point of bifurcation of the fixed points; see Figure 7(B).

To have a one-dimensional map, we need one of the jumps of the trajectory from the left to right branches or from the right to left branches of the nullclines to occur through a saddle-node bifurcation (where the value of s_1 is known) and the other to occur instantaneously when s_2 jumps between 1 and s_{2min} (where the value of s_1 will be defined as a fixed point of the map). Therefore, we shall establish the existence of the periodic solution which follows the subcases (c) and (a') above. Namely, the trajectory will jump from the left to the right branches through the bifurcation point s_L^{off} , i.e., s_1 and s_2 known, and from the right to the left branches when s_2 jumps down from 1 to s_{2min} , i.e., s_2 known and s_1 to be determined by the map; see Figure 12.

Recall that $s(t) = s_1(t) * s_2(t)$, where we consider $s_2(t) = 1$ when $V_M \geq V_{Th(M)}$ and $s_2(t) = s_{2min}$ when $V_M < V_{Th(M)}$. When $s_{AB \rightarrow M}(t)$ jumps to 1, V_M instantaneously jumps below $V_{Th(M)}$. Thus, $s_2(t)$ instantaneously jumps to s_{2min} . However, $s_{AB \rightarrow M}(t)$ does not instantaneously jump from 1 to 0, but slowly decays with time constant $1/\tau_{M2}$. Thus, V_M requires a small amount of time, T_C , to go above $V_{Th(M)}$. In our model, we chose $V_{Th(M)}$ such that T_C is approximately $P_{AB}/20$. Hence, for one cycle of AB activity, $s_2(t) = s_{2min}$ for time $D_c P_{AB} + T_C$ and $s_2(t) = 1$ for time $(1 - D_c)P_{AB} - T_C$.

As in Case 2, we can construct a Poincaré map \mathcal{P} of an interval of s values on the right branch, $\mathcal{I} = [\tilde{s}, s_R]$, into itself. Here $s_R = s_1^R * 1$, where $s_1^R = s_R^{off}/s_{2min}$. We let $\tilde{s} = [s_1^R \exp([D_c - 1]P_{AB} + T_C)/\tau_{f1})] * 1$ so that the time distance between s_R and \tilde{s} is $[1 - D_c]P_{AB} - T_C$. Let $\tilde{s}_1 = [s_1^R \exp([D_c - 1]P_{AB} + T_C)/\tau_{f1})]$; see Figure 13.

We consider a trajectory $s_a(t)$ where $s_a(0^-) = s_1^R * s_2(0^-)$ and the trajectory is on the right branch of the nullclines. Let $s_{AB \rightarrow M}(0^-) = 0$ and $s_{AB \rightarrow M}(0^+) = 1$ so that $s_2(0^-) = 1$ and $s_2(0^+) = s_{2min}$. Thus the trajectory jumps back to the left branch at $t = 0^+$ when s_2 jumps from 1 to s_{2min} . We then choose $\tau_{r1}(j) = ((j + D_c)P_{AB} + T_C)/\ln([1 - s_1^R]/[1 - s_L^{off}])$ which guarantees that $s_a((j + D_c)P_{AB} + T_C) = s_L^{off}$ so that the trajectory which starts at s_R at $t = 0^-$ will leave the left branches of the nullclines through the bifurcation point s_L^{off} at $t = (j + D_c)P_{AB} + T_C$. Using the same argument as in Case 2 with an equivalent condition on τ_{r1} as in (25), the trajectory $s_b(t)$ with initial condition $s_b(0) = \tilde{s}_1 * s_2(0)$ will be forced to reach s_L^{off} at a time T_1 bounded between $(j + D_c)P_{AB} + T_C$ and $(j + 1)P_{AB}$. Therefore, any trajectory with $s(0) \in \mathcal{I}$ will also reach s_L^{off} during these times.

Next, we choose $\tau_{f1}(k)$ so that $s_a(t)$ gets mapped back to \mathcal{I} , particularly to \tilde{s} at the instant before $s_{AB \rightarrow M}(t)$ jumps from 0 to 1. Therefore, we let $\tau_{f1}(k) = [[k + [1 - D_c]]P_{AB} - T_C]/\ln(s_1^L/\tilde{s}_1)$. Thus, at $s_a(T_2^-)$, where $T_2 = (k + j + 1)P_{AB}$, $s_a(t)$ lies in \mathcal{I} . In a similar argument to that of Case 2, the trajectory $s_b(t)$ with $s_b(0) = \tilde{s}_1 * s_2(0)$ and $s_b((j+1)P_{AB}) = s_L^{off}$ will also lie in \mathcal{I} at $t = T_2^-$ with $\tilde{s} = s_a(T_2^-) < s_b(T_2^-) < s_R$.

We define a one-dimensional Poincaré map $\mathcal{P} : \mathcal{I} \rightarrow \mathcal{I}$ where $\mathcal{P}(s) = s(T_2)$. The argument showing that \mathcal{P} is a contraction mapping on \mathcal{I} is the same as in Case 2. Consequently, there exists a locally unique, asymptotically stable value $s_{Case\ 3}^* \in \mathcal{I}$ such that $\mathcal{P}(s_{Case\ 3}^*) = s_{Case\ 3}^*$.

Remark. The periods of the constructed solutions in Cases 2 and 3 are both $(j+k+1)P_{AB}$. Note that this occurs since the values of $\tau_{r1}(j)$ and $\tau_{f1}(k)$ are chosen to be different in both cases. In general, if, a priori, τ_{r1} is chosen to have the same value for both Cases 2 and 3, and

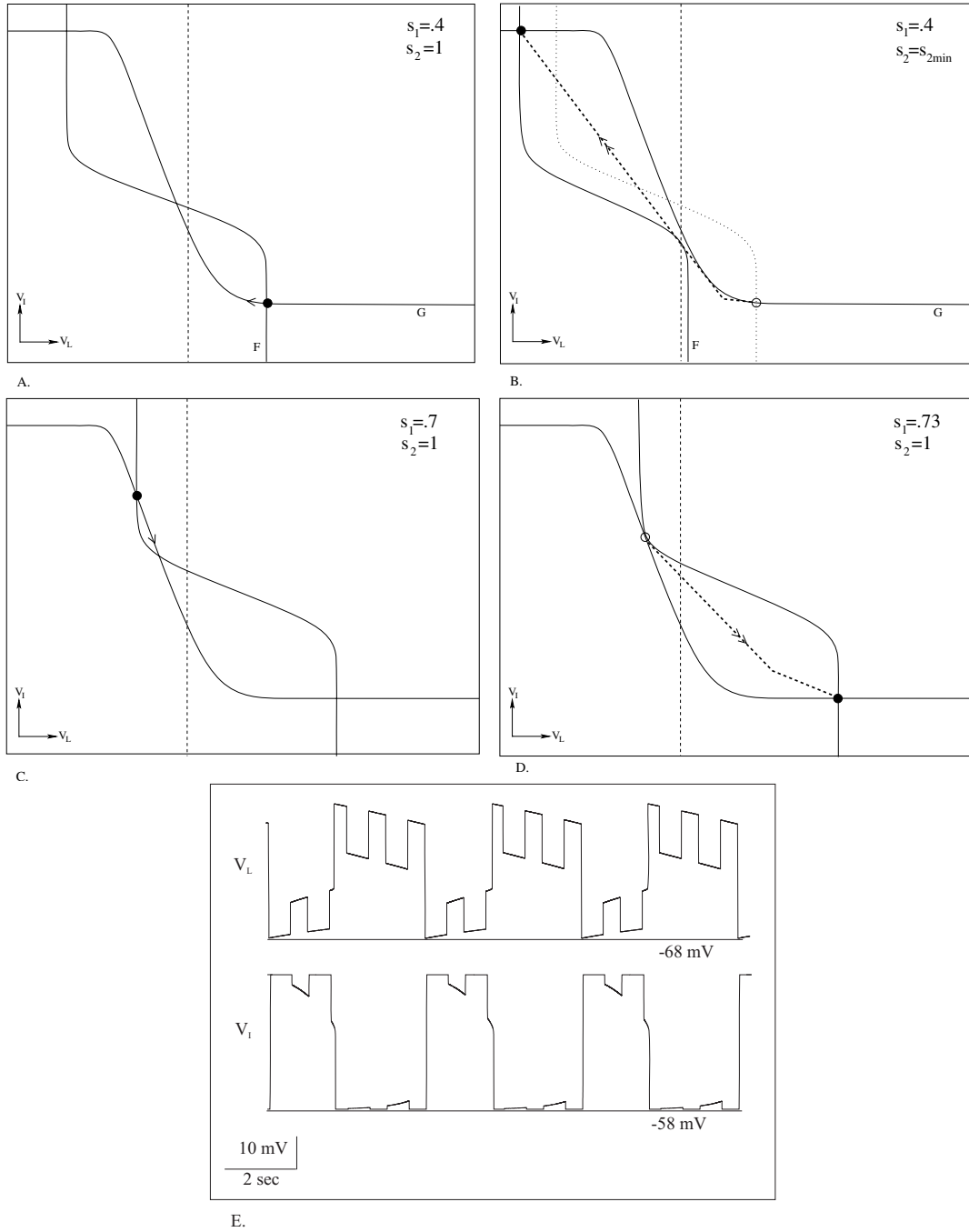


Figure 12. Case 3 solution trajectory and nullclines. (A) The trajectory lies at the stable fixed point (\bullet) on the right branches of the nullclines where $s_{AB \rightarrow I} = 0$ and $s_2 = 1$. (B) When s_2 jumps to s_{2min} , s instantaneously goes below s_R^{off} and the fixed point is lost. Thus, the solution trajectory is forced to jump to the stable fixed point on the left branches of the nullclines (shown by the dashed line with double arrows). (C)–(D) On the left branches of the nullclines, the fixed point is lost while $s_2 = 1$ and s_1 becomes large enough for the saddle-node bifurcation to occur through s_L^{off} . Now, the solution trajectory is forced to jump to the right branches of the nullclines. (E) Voltage traces of LG and Int1 for s satisfying the above conditions.

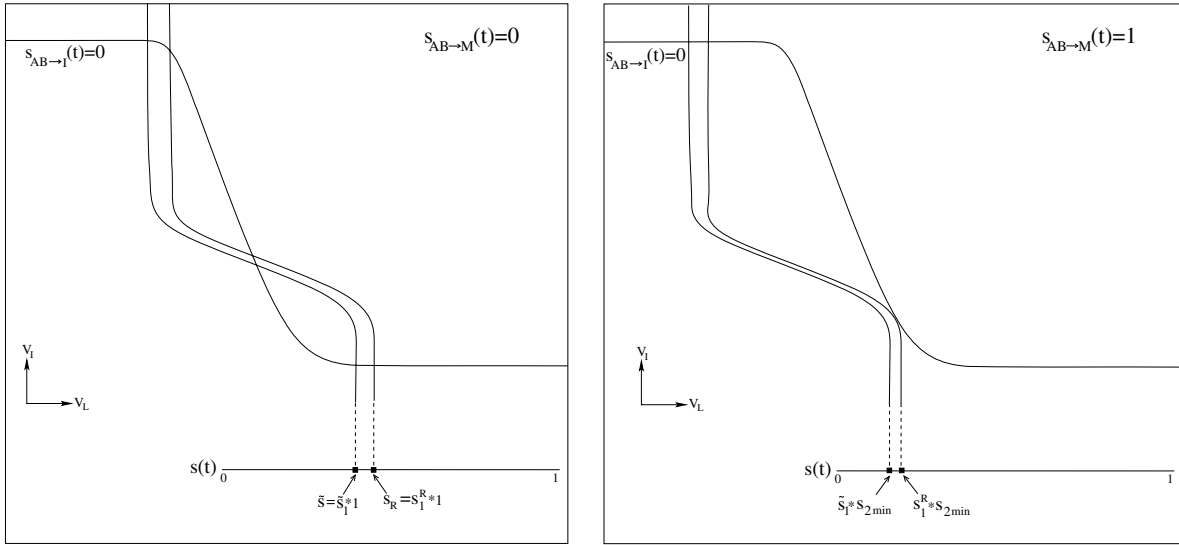


Figure 13. (A) To define the Poincaré map for Case 3, we let $I = [\tilde{s}, s_R]$ where $s_R = s_1^R * 1$, $s_1^R = s_1^{off} / s_{2min}$, and $\tilde{s} = [s_1^R \exp([D_c - 1]P_{AB} + T_C) / \tau_{f1}] * 1$. (B) For $s = s_R$, when s_2 jumps from 1 to s_{2min} , s jumps to $s_1^R * s_{2min}$. Similarly, for $s = \tilde{s}$, when s_2 jumps to s_{2min} , s jumps to $\tilde{s}_1 * s_{2min}$.

similarly for τ_{f1} , then the periods of Cases 2 and 3 need not be the same.

Case 4: Rhythmic MCN1 excitation with AB input to Int1 present. In Case 4, the MCN1 to LG excitation is rhythmic ($\bar{g}_{AB \to M} > 0$) and AB inhibits Int1 ($\bar{g}_{AB \to I} > 0$). Consequently, the V_L nullcline shifts to the right and left with slow changes in s_1 and with quick jumps of s_2 between 1 to s_{2min} . The V_I nullcline jumps up and down instantaneously due to the $s_{AB \to I}$ oscillations between 0 and 1.

Suppose the trajectory lies at the stable fixed point on the left branches of the V_L and V_I nullclines. Here, $V_L < V_T$ which allows s_1 to increase. When $s_{AB \to M}(t) \rightarrow 1$, the V_L nullcline jumps to the left. Similarly, when $s_{AB \to I}(t) \rightarrow 1$, the V_I nullcline jumps down. Recall that the time difference between when the V_L and V_I nullclines shift is controlled by the parameter m . For example, if $m = 0$, the V_L nullcline jumps to the left at the same time that the V_I nullcline jumps down. However, if $m = D_c P_{AB}$, then when the V_L nullcline jumps to the left, the V_I nullcline jumps up. This creates several possibilities for the length of the period.

To provide more insight into the role of m , suppose again that $m = 0$. In Case 2, the jumping down of the V_I nullcline allowed the fixed point to bifurcate at smaller values of s_1 relative to Case 1. However, in Case 4 for $m = 0$, whenever the V_I nullcline jumps down, the V_L nullcline jumps back to the left. If this jump to the left is large enough ($1 - s_{2min}$ is large) and the jump down in the V_I nullcline is not extremely large, there will still exist a stable fixed point on the left branches. In this case, the trajectory will have to wait until $s_2 = 1$ and s_1 has grown large enough so that the fixed point occurs where the nullclines intersect tangentially for $s_{AB \to I}(t) = 0$ (Figure 7A) or when s_2 jumps to 1 ($s_{AB \to M}(t)$ jumps to 0) and the fixed point is instantaneously lost (Figure 7B). This is equivalent to (a') and (c') in Case 3. If the jump to the left of the V_L nullcline is not large and/or the jump down in the V_I nullcline is extremely large, the fixed point will be lost and the trajectory will immediately jump to

the stable fixed point on the right branches of the nullclines. This is equivalent to Case 2. The above result also extends to the situation in which $m \in (0, T_C]$ (where T_C is the time it takes for V_M to increase under (11) and (13) from V_M^* to $V_{TH(M)}$) because for $0 < m \leq T_C$, each time the V_I nullcline is in the downward position, the V_L nullcline is shifted to the left. Therefore, the fixed point cannot be lost until s_1 grows large enough for the bifurcation to occur while $s_2 = 1$.

Next suppose that $m = D_c P_{AB}$. For $m = D_c P_{AB}$, each time the V_I nullcline is shifted in the downward position, the V_L nullcline remains to the right. Therefore, as opposed to the situation in which $m = 0$, the fixed point on the left branches of the nullclines can be lost due to the jump down of the V_I nullcline as in Case 2; see Figure 7C. This same idea extends to values of m lying in a neighborhood, $[R_1, R_2]$, of $D_c P_{AB}$ where $R_1 > T_C$, $R_2 < P_{AB}$. For $m \in [R_1, R_2]$, there is always some amount of time for which the V_L nullcline is to the right while the V_I nullcline is shifted downward, thus allowing the fixed point to be lost at an earlier time than in Case 3.

We now consider the existence of a periodic solution for Case 4 with $\tau_{r1}(j)$ and $\tau_{f1}(k)$ defined as in Case 3. For $m \in (0, T_C]$, the periodic orbit will be defined in exactly the same way as Case 3. Consider the interval \mathcal{I} on the right branches as defined in Case 3 with $s_{AB \rightarrow M}(0^-) = 0$ and $s_{AB \rightarrow M}(0^+) = 1$. Let $s_a(t)$ be a trajectory with $s_a(0) = s_1^R * s_2(0)$. At $t = 0^+$, $s_{AB \rightarrow M}$ jumps to 1 and $s_{AB \rightarrow I}$ remains equal to 0 because of the small delay m . Thus, s_2 instantaneously jumping to s_{2min} forces the trajectory to the left branches in the same way as Case 3 because the V_I nullcline remains in the upward position at $t = 0^+$.

On the left branches with $m \in (0, T_C]$, each time $s_{AB \rightarrow I} = 1$, pushing the V_I nullcline down, $s_2 = s_{2min}$ and the V_L nullcline is forced to the left. Thus, the trajectory with initial conditions as stated above cannot jump from s_L^{on} as in Case 2 because each time the V_I nullcline is in its downward position, the V_L nullcline is shifted too far to the left for s to reach s_L^{on} . Therefore, the only time at which the fixed point of the left branches can be lost is when $s_2 = 1$. At $t = (j + D_C)P_{AB}$, $s_{AB \rightarrow M}(t)$ will jump to 0. However, s_2 will not jump to 1, returning the V_L nullcline to the right, until $t = (j + D_C)P_{AB} + T_C$. Hence, at $t = (j + D_C)P_{AB} + T_C$, $s_{AB \rightarrow I}$ will already be equal to 0 since $m \leq T_C$ and the trajectory will reach s_L^{off} tangentially as in Case 3. By choosing $\tau_{f1}(k)$ as in Case 3, $s_a(t)$ gets mapped to \tilde{s} at $t = T_2^-$.

With the same argument as in Case 3, the trajectory $s_b(t)$ with $s_b(0) = \tilde{s}_1 * s_2(0)$ and $s_b(T_1) = s_L^{off}$ (where $T_1 \in ((j + D_c)P_{AB} + T_C, (j + 1)P_{AB} + T_C)$) will also be mapped back to \mathcal{I} at $t = T_2^-$ with $\tilde{s} = s_a(T_2^-) < s_b(T_2^-) < s_R$. Therefore, the one-dimensional Poincaré map $\mathcal{P} : \mathcal{I} \rightarrow \mathcal{I}$ where $\mathcal{P}(s) = s(T_2)$ is established exactly as in Case 3. Thus for $m \in (0, T_C]$, the same arguments apply to show that there exists a unique, asymptotically stable periodic orbit in Case 4, and the periodic orbits of Cases 3 and 4 have the same period.

For $m \in [R_1, R_2]$, the period of the solution trajectories in Case 4 is locked to the period of AB oscillations and is, therefore, much shorter than the period of solution trajectories in Case 3. For $m \in [R_1, R_2]$, as stated above, on the left branches of the nullclines, the inhibition from AB to $MCN1$ and to $Int1$ is timed such that while the V_I nullcline is shifted downward, $s_2 = 1$ which places the V_L nullcline to the right. Thus, s_1 does not need to grow very large for the LG interburst to end. Once on the right branches, the burst of LG is ended during the first time s_2 jumps to s_{2min} because s_1 is sufficiently small (due to the fact that the LG

interburst was ended for a small value of s_1) to push the V_L nullcline far enough to the left to cause a loss in the fixed point. Similarly, once the solution trajectory is back to the left branches, s_1 is large enough (because s_1 did not decay a long time on the right branches) so that the first jump in s_2 back to 1 causes a loss of the fixed point and an end to the LG interburst. In the regions $T_C < m < R_1$ and $R_2 < m \leq P_{AB}$, the solution trajectories remain periodic but are slightly more complicated to describe than those outside of these regions. For example, with the parameters fixed as above, when $m \in (0, T_C]$ or $m \in [R_1, R_2]$ consecutive LG bursts have exactly the same length as do consecutive $Int1$ bursts. However, when m is not in these regions, consecutive LG bursts and consecutive $Int1$ bursts need not have the same length. Instead, several cycles of LG and $Int1$ oscillations may be required before the LG (and $Int1$) burst duplicates its length. We further explain this in the next section.

4. Determining the frequency of solutions. The period of the gastric mill rhythm can be computed as the sum of the LG burst and the LG interburst. During the interburst, s_1 increases toward a maximum value which we shall denote s_{max} . Similarly, during the burst, s_1 decreases toward a minimum value s_{min} . The periodic solutions in Cases 1–4 are then computed by finding out how much time is needed for s_1 to evolve between the values of s_{max} and s_{min} on the left (during the interburst) and right (during the burst) branches. Using (7), it is straightforward to see that

$$(32) \quad P = \tau_{r1} \ln \left(\frac{1 - s_{min}}{1 - s_{max}} \right) + \tau_{f1} \ln \left(\frac{s_{max}}{s_{min}} \right).$$

The main question now is to determine the values s_{min} and s_{max} for each of the four cases. However, these values have already been determined in the construction of the periodic solutions above. In particular, for Case 1, $s_{min} = s_R^{off}$ and $s_{max} = s_L^{off}$. For Case 2, $s_{min} = s_{Case\ 2}^*$ and $s_{max} = s_L^{on}$. Note that $s_L^{on} < s_L^{off}$. Since the AB inhibition does not affect the right branches of the V_I nullcline too much, $s_{Case\ 2}^* \approx s_R^{off}$. Thus from (32), it is seen that the period of Case 2 is smaller than the period of Case 1 since the interburst of LG is shorter. This result is consistent with what was found by Manor et al. [16].

In Case 3, $s_{min} = s_{Case\ 3}^*$ and $s_{max} = s_L^{off}$. Here $s_{Case\ 3}^* \in [s_1^R \exp([(D_c - 1)P_{AB} + T_C]/\tau_{f1}), s_1^R]$. Finally, for Case 4, when $m \in (0, T_C]$, the periodic solution is different than the one constructed in Case 3 due to the shifting of the V_I nullcline. However, the period of the solutions in Cases 3 and 4 are the same because the values of s_{min} and s_{max} are the same. When $m > T_C$, $s_{min} \in [s_1^R \exp([(D_c - 1)P_{AB} + T_C]/\tau_{f1}), s_1^R]$ and $s_{max} \in [s_L^{on}, 1 + (s_L^{on} - 1)\exp(-(D_C P_{AB} + T_C)/\tau_{r1})]$. Calculations of s_L^{off} , s_R^{off} , s_L^{on} , and s_R^{on} can be found in the appendix. Using (32), we calculated values for the period for Cases 1 through 4. The analytic results are shown in Table 1 for Cases 1 through 3. There, we assumed for Case 2 that $s_{min} = s_{Case\ 2}^*$ equals the average of s_R^{off} and s_R^{on} , while for Case 3, $s_{min} = s_{Case\ 3}^* = s_R^{off}/s_{min}$.

To confirm the validity of our analytic computations of the period using (32), we also numerically solved the set of equations in our model using XPP [11]. See the appendix for parameter values. For Cases 1 through 3, these results are also given in Table 1 and show a close correlation between the calculation of the periods obtained analytically and numerically.

In Figure 14, we show the results of numerically calculating the period in Case 4 as a function of the delay parameter m with $\tau_{r1} = 7200$ and $\tau_{f1} = 5500$. We see that for

Table 1

A comparison of the analytic versus numerical determinations of period in Cases 1–3.

Period calculation for $\tau_{r1} = 4900$ msec, $\tau_{f1} = 4000$ msec		
Case	XPP simulation	Analytic formula
Case 1	period=10,140 msec	period=10,075 msec
Case 2	period=5,000 msec	period=4,688 msec
Case 3	period=4,000 msec	period=3794 msec

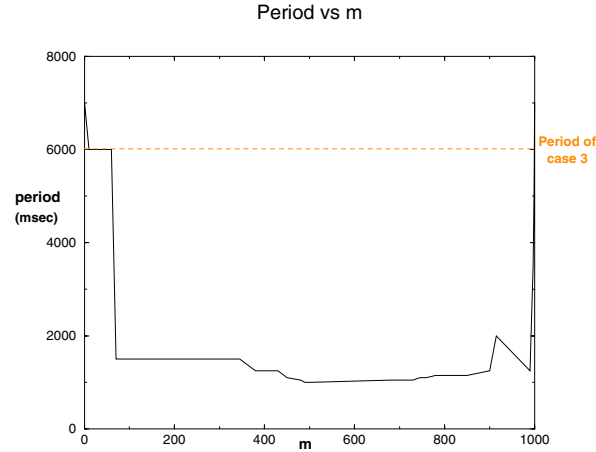


Figure 14. The period of the gastric mill cycle is plotted for different delays, m , in Case 4. The period of Case 3 is marked by the dashed line. There is a small range of delays, $0 < m \leq 60$, for which the period of the gastric mill rhythm is equal for Cases 3 and 4.

$0 < m \leq 60$, the period of the gastric mill rhythm for Case 3 is equal to that of Case 4. For $470 < m \leq 740$, the period of the gastric mill is equal to the period of AB activity. For $60 < m \leq 470$, there is a transition between having a period equal to that of Case 3 to the much shorter period of AB activity. Similarly, for $740 < m \leq 1000$, the period begins to increase from 1 sec up to the period found in Case 3. As stated in the previous section, for $60 < m \leq 470$ and for $740 < m \leq 1000$, it may take several cycles of LG and $Int1$ oscillations before the LG and $Int1$ burst lengths duplicate themselves where $R_1 = 470$ and $R_2 = 740$. In these situations, the period is calculated as the time it takes to have two duplicate LG burst lengths divided by the number of cycles of LG oscillations occurring in that time. Figure 15 shows the gastric mill rhythm frequency as found in experiments by Wood et al. [30] for Cases 1–4. In this work, Wood et al. [30] artificially replicate the effect of AB activity on $MCN1$ through computer controlled stimulation of $MCN1$. We see that for $MCN1$ tonic, the frequency of the network is much higher when the AB input to $Int1$ is present. For $MCN1$ rhythmic, the frequency of the network is higher than when $MCN1$ is tonic; however, there is no change in frequency when the AB input to $Int1$ is added to the network. Figure 16 shows that our model accurately replicates the behavior of the actual gastric mill when $0 < m \leq 60$. Thus, the time mismatch between the pyloric and modulatory inputs to the gastric mill network is critical in establishing the correct frequency of the system.

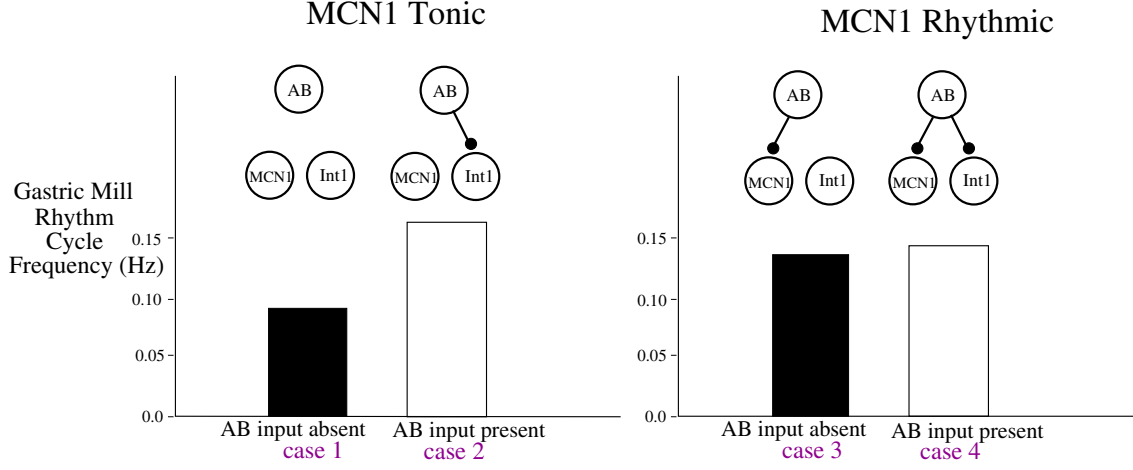


Figure 15. Experimental findings of the gastric mill rhythm cycle frequency for Cases 1–4 [30].

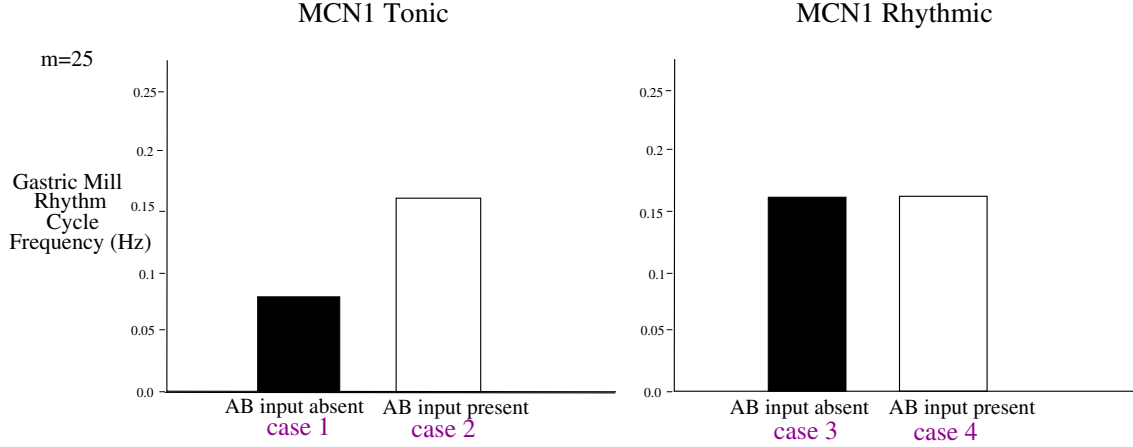


Figure 16. Calculations of the gastric mill rhythm cycle frequency for Cases 1–4 using our model with $\tau_{r1} = 7200\text{msec}$, $\tau_{f1} = 5500\text{msec}$, $\tau_{r2} = 1\text{msec}$, $\tau_{f2} = 1\text{msec}$, period of $s_{AB} = 1\text{sec}$, $m = 25\text{msec}$, and $\bar{g}_s = 6\text{mS/cm}^2$ in Cases 1 and 2 and $\bar{g}_s = 7\text{mS/cm}^2$ in Cases 3 and 4.

5. Voltage dependent MCN1 to LG synapse. We now consider the effect of having voltage dependent coupling between *MCN1* and *LG* as opposed to a constant conductance synapse. Therefore, we return to (1) with $g_s(V_L) = \bar{g}_s s_\infty(V_L)$, where $s_\infty(V_L)$ is a sigmoidal gating function varying between 0 and 1 of the form

$$(33) \quad s_\infty(V) = \left(1 + \exp \frac{v_k - V_k}{k} \right)^{-1}.$$

Due to this voltage dependency, the amount of excitation that *LG* receives from *MCN1* will depend upon the voltage of *LG* causing *LG* to receive less excitation when it, itself, is at a low voltage. Thus, when *LG* is in its interburst, the strength of the synapse will be weaker than in the voltage independent case. When *LG* is in its burst, the strength of the synapse

will increase to a value near to that of the previous section. As a consequence of the weaker conductance, in all of the Cases 1–4, the voltage dependency will increase the LG interburst duration because s will be required to grow to a larger value of s_{max} for the fixed point to be lost on the left branches of the nullclines. On the right branches of the nullclines, where LG is in its burst, $s_\infty(V_L)$ is closer to 1, and, therefore, the burst duration of LG will not be directly affected as significantly as the interburst duration. However, the value of s_{min} will be slightly larger than when the conductance is not voltage dependent because as V_L decreases on the right branches, s_∞ also decreases. Therefore, s will not need to decrease as much to cause a loss of the fixed point and an end to the LG burst. The increase in the interburst duration in all Cases 1–4, however, is larger than the decrease in burst duration, resulting in an increase in the period of the solutions.

Upon relaxing the conditions that s_2 and $s_{AB \rightarrow I}$ jump between their minimum and maximum values instantaneously, in addition to increasing the period in Cases 1–4, the voltage dependency also increases the range of m over which the period of Case 3 equals the period of Case 4. When the rise and fall of s_2 is not instantaneous but occurs on the slow timescale, s_2 moves continuously between its maximum and minimum values. Regardless of whether the conductance of the $MCN1$ synapse to LG is constant or voltage dependent, the same condition must be satisfied for the period of Case 3 to equal the period of Case 4. This condition is that the fixed point on the left branches of the nullclines must be lost through s_L^{off} . That is, m must be chosen to live in a certain interval, say, $[M_1, M_2]$, such that once s_1 has grown large enough for s to reach s_L^{on} while $s_{AB \rightarrow I} = 1$, the V_L nullcline must be shifted far enough to the left by s_2 when $s_{AB \rightarrow M} = 1$ so that the saddle-node bifurcation does not occur at s_L^{on} . This situation persists until m becomes just larger than M_2 . For $M_2 < m < D_c P_{AB}$, when $s_{AB \rightarrow I}$ jumps to 1, $s_{AB \rightarrow M}$ will already equal 1 so the V_L nullcline will already be to the left. However, before $s_{AB \rightarrow I}$ returns 0, $s_{AB \rightarrow M}$ will return 0. Consequently, the V_L nullcline will move to the right and the fixed point will not be lost through s_L^{on} .

When s_2 changes on the slow timescale and m is slightly too large as described above, the loss of the fixed point through s_L^{on} often occurs while s_2 is increasing toward 1 but has not yet reached its maximum value of 1. As a specific example, for $\tau_{r1} = \tau_{f1} = 4000$, $\tau_{r2} = \tau_{f2} = 325$, and conductance of the $MCN1$ to LG synapse constant ($s_\infty(V_L) = 1$), the periods of Cases 3 and Cases 4 are the same for $80 \leq m \leq 275$. Note that the lower bound on the interval is 80 (not 0) since we have relaxed the condition that s_2 and $s_{AB \rightarrow I}$ change instantaneously. Once $m > 275$, the saddle-node bifurcation occurs through s_L^{on} instead of s_L^{off} , thus causing the period of Case 4 to be smaller than the period of Case 3.

Now let us consider the effect of the voltage dependent conductance on the position of the V_L nullcline and, therefore, the role it plays in altering the interval of m over which the period in Case 3 equals that in Case 4. When LG is at a low voltage, $s_\infty(V_L)$ is close to 0. Thus, on the left branches of the nullclines, when s_2 decreases to its minimum, there is a much larger jump to the left of the V_L nullcline than when the conductance is constant. Furthermore, even as s_2 increases back to 1, the V_L nullcline remains significantly far to the left until s_2 gets very close to 1. Therefore, even as m increases to the range $[M_2, D_c P_{AB}]$ where $s_{AB \rightarrow M}$ jumps back to 0 (forcing s_2 to increase back to 1) just before $s_{AB \rightarrow I}$ returns to 0, the V_L nullcline will remain too far to the left (because it takes some amount of time for s_2 to grow close enough to 1) for the saddle-node bifurcation to occur at s_L^{on} . Hence, the fixed point cannot

be lost through s_L^{on} while s_2 is growing toward 1, as occurs when the conductance is constant. Furthermore, when $s_{AB \rightarrow I}$ is a half-sine function as in Manor et al. [16], the V_I nullcline spends less time in the downward position. Consequently, there is again a smaller range of time for s to reach s_L^{on} when the V_I nullcline is in the downward position. Accordingly, a larger interval of m will exist for the fixed point on the left branches of the nullclines to be lost from s_L^{off} as in Case 3 when the conductance is voltage dependent than when the conductance is constant. Returning to the example in the above paragraph but now allowing the conductance of the *MCN1* to *LG* synapse to be voltage dependent, the interval of m for which the period of Case 3 equals the period of Case 4 extends to $80 \leq m \leq 350$. When s_2 has instantaneous kinetics, there is no significant difference in the range of m between the voltage dependent and non-voltage dependent cases because s_2 is always equal to either 1 or 0 so the fixed point on the left branches cannot be lost while s_2 is increasing toward 1.

6. Discussion. Networks involved in the generation of rhythmic movements often involve sets of reciprocally inhibitory neurons that rely on external stimuli to trigger oscillations or to set the appropriate frequency of the rhythm [2, 6, 25]. It has been observed that while tonic stimulation may often be sufficient to elicit the network activity, the synaptic inputs driving these circuits are themselves rhythmic [5, 29]. An example of this is the pyloric network of the lobster stomatogastric nervous system which receives rhythmic excitatory input. The same effects of this rhythmic input, however, can be achieved through tonic firing of the input cells [19].

Furthermore, it has been noted in many cases that although one source of input is sufficient to produce oscillations in the target network, multiple inputs act together to generate and set the frequency of the network. The heartbeat of the leech, for example, is controlled by pairs of reciprocally inhibitory neurons. These oscillators receive inhibitory input from interneurons that act to coordinate the activity of the separate oscillators [7]. Einum and Buchanan [10] also recently showed that reticulospinal neurons of the lamprey brain stem receive both excitatory and inhibitory rhythmic inputs from neurons in the spinal cord during locomotor activity.

The stomatogastric nervous system of the crab, made up of an asymmetric half-center oscillator, provides a nice example of a system that receives multiple rhythmic synaptic inputs in order to oscillate. The interactions between the gastric mill network and pyloric network have been extensively studied to show how each network acts to influence one another's frequency [3, 4, 28]. In their work, Nadim et al. [21] and Manor et al. [16] considered how the frequency of the gastric mill rhythm is generated and controlled in the presence of both a slow modulatory input and a much faster periodic input.

In this paper, we continued upon the work of Nadim et al. [21] and Manor et al. [16] with the aim of mathematically explaining the experimental results of Wood et al. [30]. Specifically, we addressed the effect of having a rhythmic modulatory input versus a tonic input drive the network oscillations and then how two simultaneous rhythmic inputs work together to determine the network frequency. In order to do this, we incorporated the rhythmicity of the modulatory projection neuron on the existing model of Manor et al. [16]. We then derived conditions on the parameters that dictate the strength and rise and decay rates of the synaptic currents to ensure the existence, local uniqueness, and stability of periodic solutions. Once periodic orbits were established, we derived a formula to estimate the period of such orbits

in the presence and absence of pyloric input to the gastric mill network for both tonic and rhythmic modulatory input.

Using geometric, singular perturbation theory, the multidimensional system is reduced to studying the position of the nullclines in the $V_L - V_I$ phase plane with the variable controlling the amount of excitation provided from the modulatory projection neuron to the gastric mill treated as a parameter. The model shows that the rhythmicity of the projection neuron speeds the gastric mill rhythm by allowing the loss of a relevant stable fixed point to occur at an earlier time than when the input is tonic. Thus, although tonic stimulation of the gastric mill network can generate the gastric mill rhythm, the rhythmicity of the input speeds the frequency of the gastric mill rhythm as in seen by Wood et al. [30].

In the presence of the rhythmic modulatory excitation and fast pyloric inhibition, the timing of the jump of the V_L and V_I nullclines in response to the AB input to $Int1$ and to $MCN1$ determines how the loss of the stable fixed point on either the left or right branches of the nullclines will occur. This, in turn, determines the length of the LG and $Int1$ interburst and burst durations. The frequency calculated from this model matches the experimental results of Wood et al. [30] only when there is either a short delay or no delay in the timing of the two pyloric inputs. In this case, the position of the V_L nullcline in response to the AB inhibition of $MCN1$ prevents the AB disinhibition of LG from ending the LG interburst. Thus, it is as if there is only one source of synaptic input to the gastric mill network. Therefore the analysis gives a possible biological mechanism by which the effect of the two simultaneous synaptic inputs can overlap to result in a frequency equivalent to that of having only one of the inputs present. If the delay is chosen differently, however, the gastric mill rhythm has a higher frequency than when only one of the inputs is present because the position of the V_L nullcline does not prevent LG from getting disinhibited by AB . Thus, the timing of the inputs can be used as a tool to switch between different modes of firing frequency. This may serve as a means by which different chewing patterns are elicited.

The biological and mathematical reductions of the full, compartmental model of Nadim et al. [21] implemented by Manor et al. [16] and extended to this work have proven to be instrumental in understanding the frequency regulation of the gastric mill rhythm and intercircuit coordination with the pyloric network. The reduced model neglects all intrinsic currents and models the neurons in this network as having only leak currents. Despite the severity of the reductions, the reduced network is able to accurately model the gastric mill rhythm and its response to the slow, modulatory, and fast pyloric inputs. In [1], Ambrosio shows that the results found through analysis of the reduced model do extend to the full model. The reduced model also clarifies the relationship between the synaptic rise and decay times of the AB inhibition of $MCN1$ in the full model necessary to obtain the experimentally observed behavior. Furthermore, because the reduced model consisting of passive neurons is able to accurately reproduce the qualitative behavior of the full model, it is clear that the synaptic currents and their timing with respect to one another are the primary components responsible for the dynamics of the gastric mill rhythm. This is important because the ability to ignore the intrinsic dynamics of each of the neurons results in significantly simpler equations. This makes mathematical analysis much more accessible. For example, in this network, we were able to reduce the study of our system to the study of a one-dimensional map. This then allowed us to define a Poincaré map to prove the existence and stability of periodic orbits,

which would have been much more difficult if working in higher dimensions.

Such techniques can be extended to numerous other models whose intrinsic and synaptic currents act on multiple timescales. The leech heartbeat mentioned above, for example, is controlled by a network of reciprocally inhibitory neurons that are dependent upon both synaptic and intrinsic currents. These currents exhibit both fast and slow dynamics and a biophysically detailed model of this network exists [22, 23]. Although this model was shown to accurately reproduce many of the behaviors of the real network, some properties have not yet been able to be reproduced and the significance of certain currents is not yet clearly understood. In particular, a reduced model may give some insight into the extreme sensitivity of the oscillations to the leak current parameters seen in the more detailed models. More generally, a reduced version of this model that is more amenable to mathematical investigation in terms of allowing for a reduction to lower dimensions and phase plane analysis is likely to more clearly reveal many of the underlying properties responsible for such things as the network oscillations and sensitivity to synaptic and intrinsic inputs.

Appendix A. We describe how to calculate the bifurcation points s_L^{off} , s_L^{on} , s_R^{off} , and s_R^{on} . On the left branch, when the two nullclines intersect tangentially for $s_{AB \rightarrow I}(t) = 0$, then $s = s_L^{off}$. Similarly, on the right branch when $s = s_R^{off}$ and $s_{AB \rightarrow I}(t) = 0$, the fixed point occurs when the two nullclines intersect tangentially. Thus, to calculate s_L^{off} and s_R^{off} , we use the equations for the V_L and V_I nullclines:

$$(34) \quad V_L = F(V_I, s) = \frac{g_{leak,L}E_{leak,L} + \bar{g}_{I \rightarrow L}n_\infty(V_I)E_{I \rightarrow L} + \bar{g}_s s E_{exc}}{g_{leak,L} + \bar{g}_{I \rightarrow L}n_\infty(V_I) + \bar{g}_s s}$$

and

$$(35) \quad V_I = G(V_L, s_{AB \rightarrow I}) = \frac{g_{leak,I}E_{leak,I} + \bar{g}_{L \rightarrow I}n_\infty(V_L)E_{L \rightarrow I} + \bar{g}_{AB \rightarrow I}s_{AB \rightarrow I}(t)E_{AB \rightarrow I}}{g_{leak,I} + \bar{g}_{L \rightarrow I}n_\infty(V_L) + \bar{g}_{AB \rightarrow I}s_{AB \rightarrow I}(t)}.$$

We rewrite (35):

$$(36) \quad \begin{aligned} V_L &= -k_L l n \left[-1 + \frac{\bar{g}_{L \rightarrow I}(V_I - E_{L \rightarrow I})}{-g_{leak,I}(V_I - E_{leak,I}) - \bar{g}_{AB \rightarrow I}s_{AB \rightarrow I}(t)(V_I - E_{AB \rightarrow I})} \right] + v_L \\ &\doteq \tilde{G}(V_I, s_{AB \rightarrow I}). \end{aligned}$$

We find the equation for the tangent point by solving

$$(37) \quad \frac{dF(V_I, s)}{dV_I} = \frac{d\tilde{G}(V_I, s_{AB \rightarrow I})}{dV_I}.$$

From (37), we obtain a quadratic equation for s :

$$(38) \quad \begin{aligned} &\bar{g}_s^2 s^2 + s \left[2\bar{g}_s [g_{leak,L} + \bar{g}_{I \rightarrow L}n_\infty(V_I)] - \bar{g}_{I \rightarrow L}E_{I \rightarrow L} \frac{dn_\infty(V_I)}{dV_I} g_s \frac{dV_I}{d\tilde{G}} \right. \\ &+ \left. \bar{g}_{I \rightarrow L} \frac{dn_\infty(V_I)}{dV_I} \bar{g}_s E_{exc} \frac{dV_I}{d\tilde{G}} \right] + [g_{leak,L} + \bar{g}_{I \rightarrow L}n_\infty(V_I)]^2 \\ &- \frac{dV_I}{d\tilde{G}} \left[g_{leak,L} \bar{g}_{I \rightarrow L} E_{I \rightarrow L} \frac{dn_\infty(V_I)}{dV_I} - \bar{g}_{I \rightarrow L} \frac{dn_\infty(V_I)}{dV_I} [g_{leak,L} E_{leak,L} \right. \\ &\left. + \bar{g}_{I \rightarrow L} n_\infty(V_I) E_{I \rightarrow L}] \right] = 0. \end{aligned}$$

Next, we use the restriction that the tangency of the nullclines must occur at a fixed point. Therefore, we use the equations for the V_L and V_I nullclines to determine the fixed points for different values of s . We rewrite (34) as

$$(39) \quad s = (-g_{leak,L}(V_L - E_{leak,L}) - \bar{g}_{I \rightarrow L} n_\infty(V_I)(V_L - E_{I \rightarrow L}))/g_s(V_L)(V_L - E_{exc}).$$

We then plug (36) into (39) to obtain an equation for $s = S(V_I)$. This equation says that for each value of V_I there exists a unique value of s which will cause the nullclines to intersect. We then check to see if this value of s also satisfies the quadratic equation (38). If it does, we have found a bifurcation point of the fast subsystem. There are two values of s which satisfy the equations above. The smaller valued one corresponds to s_L^{off} , and the larger corresponds to s_R^{off} . To calculate s_L^{on} and s_R^{on} , we follow the same steps as above but with $s_{AB \rightarrow I}(t) = 1$ in (35).

We used the analytically calculated values of the bifurcation points to obtain the results given in section 4. In Case 2, we assume that $s_{max} = s_L^{on}$ and s_{min} is the average of s_R^{off} and s_R^{on} . In Case 3, we assume the maximum value that s takes is s_L^{off} while $s_2 = 1$, which implies that $s_{max} = s_L^{off}$ and the minimum value s assumes is s_R^{off} when $s_2 = s_{2min}$. Therefore, s_{min} is $\frac{s_R^{off}}{s_{2min}}$. In Case 4, the values of s_{max} and s_{min} depend on m . For m near 0, for example, s_{max} and s_{min} are calculated as in Case 3. We also numerically solved (1)–(8) and (33). The parameter values used in the numerical calculations are given in Table 2.

Table 2
Parameters of the reduced model.

$g_{leak,L} = 1mS/cm^2$	$E_{leak,L} = -60mV$	$\bar{g}_{I \rightarrow L} = 5mS/cm^2$	$E_{I \rightarrow L} = -80mV$
$g_{leak,I} = .75mS/cm^2$	$E_{leak,I} = 10mV$	$\bar{g}_{L \rightarrow I} = 2mS/cm^2$	$E_{L \rightarrow I} = -80mV$
$g_{leak,M} = 2mS/cm^2$	$E_{leak,M} = 10mV$	$\bar{g}_{AB \rightarrow M} = 15mS/cm^2$	$E_{AB \rightarrow M} = -60mV$
$g_s = 4mS/cm^2$	$E_{exc} = 43mV$	$\bar{g}_{AB \rightarrow I} = .9mS/cm^2$	$E_{AB \rightarrow I} = -60mV$
$V_T = -30mV$	$v_x = -30mV$	$k_x = 4mV$	

REFERENCES

- [1] C. AMBROSIO, *The Control of Frequency of an Excitable Network Simultaneously Subjected to Multiple Oscillatory Inputs*, Ph.D. thesis, New Jersey Institute of Technology, Newark, NJ, 2005.
- [2] S. P. AIKEN, F. M. KUENZI, AND N. DALE, *Xenopus embryonic spinal neurons recorded in situ with patch-clamp electrodes—conditional oscillator after all?*, Eur. J. Neurosci., 18 (2003), pp. 333–343.
- [3] M. BARTOS, Y. MANOR, F. NADIM, E. MARDER, AND M. P. NUSBAUM, *Coordination of fast and slow rhythmic neuronal circuits*, J. Neurosci., 19 (1999), pp. 6650–6660.
- [4] M. BARTOS AND M. NUSBAUM, *Intercircuit control of motor pattern modulation by presynaptic inhibition*, J. Neurosci., 17 (1997), pp. 2247–2256.
- [5] M. J. BOURQUE AND A. KOLTA, *Properties and interconnections of trigeminal interneurons of the lateral pontine reticular formation in the rat*, J. Neurophys., 86 (2001), pp. 2583–2596.
- [6] R. L. CALABRESE, *Oscillations in motor pattern-generating networks*, Curr. Opin. Neurobiol., 5 (1995), pp. 816–823.
- [7] R. CALABRESE, F. NADIM, AND O. OLSEN, *Heartbeat control in the medicinal leech: A model system for understanding the origin, coordination, and modulation of rhythmic motor patterns*, J. Neurobiol., 27 (1995), pp. 390–402.

- [8] M. J. COLEMAN, P. MEYRAND, AND M. P. NUSBAUM, *A switch between two modes of synaptic transmission mediated by presynaptic inhibition*, *Nature*, 378 (1995), pp. 502–505.
- [9] M. J. COLEMAN AND M. P. NUSBAUM, *Functional consequences of compartmentalization of synaptic input*, *J. Neurosci.*, 14 (1994), pp. 6544–6552.
- [10] J. F. EINUM AND J. T. BUCHANAN, *Reticulospinal neurons receive direct spinobulbar inputs during locomotor activity in lamprey*, *J. Neurophys.*, 92 (2004), pp. 1384–1390.
- [11] B. ERMENTROUT, *Simulating, Analyzing, and Animating Dynamical Systems: A Guide to XPPAUT for Researchers and Students*, Software Environ. Tools 14, SIAM, Philadelphia, 2002.
- [12] S. GRILLNER AND T. MATSUSHIMA, *The neural network underlying locomotion in lamprey—synaptic and cellular mechanisms*, *Neuron*, 7 (1991), pp. 1–15.
- [13] S. GRILLNER AND P. WALLEN, *Central pattern generators for locomotion, with special reference to vertebrates*, *Ann. Rev. Neurosci.*, 8 (1985), pp. 233–261.
- [14] O. KIEHN AND O. KJAERULFF, *Distribution of central pattern generators for rhythmic motor outputs in the spinal cord of limbed vertebrates*, *Ann. NY Acad. Sci.*, 860 (1998), pp. 110–129.
- [15] S. P. LIESKE, M. THOBY-BRISSON, P. TELGKAMP, AND J. M. RAMIREZ, *Reconfiguration of the neural network controlling multiple breathing patterns: Eupnea, sighs and gasps*, *Nat. Neurosci.*, 3 (2000), pp. 600–607.
- [16] Y. MANOR, F. NADIM, S. EPSTEIN, J. RITT, E. MARDER, AND N. KOPELL, *Network oscillations generated by balancing graded asymmetric reciprocal inhibition in passive neurons*, *J. Neurosci.*, 19 (1999), pp. 2765–2779.
- [17] E. MARDER AND D. BUCHER, *Central pattern generators and the control of rhythmic movements*, *Curr. Biol.*, 11 (2001), pp. R986–R996.
- [18] E. MARDER AND R. L. CALABRESE, *Principles of rhythmic motor pattern generation*, *Physiol. Rev.*, 76 (1996), pp. 687–717.
- [19] J. MILLER AND A. SELVERSTON, *Mechanisms underlying pattern generation in lobster stomatogastric ganglion as determined by selective inactivation of identified neurons. IV. Network properties of pyloric system*, *J. Neurophys.*, 48 (1982), pp. 1416–1432.
- [20] E. MISHCHENKO AND N. ROZOV, *Differential Equations with Small Parameters and Relaxation Oscillations*, Plenum Press, New York, 1980.
- [21] F. NADIM, Y. MANOR, M. P. NUSBAUM, AND E. MARDER, *Frequency regulation of a slow rhythm by a fast periodic input*, *J. Neurosci.*, 18 (1998), pp. 5053–5067.
- [22] F. NADIM, O. H. OLSEN, E. DE SCHUTTER, AND R. L. CALABRESE, *Modeling the leech heartbeat elemental oscillator I. Interactions of intrinsic and synaptic currents*, *J. Comput. Neurosci.*, 2 (1995), pp. 215–235.
- [23] O. H. OLSEN, F. NADIM, AND R. L. CALABRESE, *Modeling the leech heartbeat elemental oscillator II. Exploring the parameter space*, *J. Comput. Neurosci.*, 2 (1995), pp. 237–257.
- [24] M. P. NUSBAUM AND M. P. BEENHAKKER, *A small-systems approach to motor pattern generation*, *Nature*, 417 (2002), pp. 343–350.
- [25] R. A. SATTERLIE, *Reciprocal inhibition and postinhibitory rebound produce reverberation in a locomotor pattern generator*, *Science*, 229 (1985), pp. 402–404.
- [26] D. SOMERS AND N. KOPELL, *Rapid synchronization through fast threshold modulation*, *Biol. Cyber.*, 68 (1993), pp. 393–407.
- [27] P. S. G. STEIN, S. GRILLNER, A. I. SELVERSTON, AND D. G. STUART, EDs., *Neurons, Networks, and Motor Behavior*, MIT Press, Cambridge, MA, 1997.
- [28] J. B. THUMA, L. G. MORRIS, A. L. WEAVER, AND S. L. HOOPER, *Lobster (*Panulirus interruptus*) pyloric muscles express the motor patterns of three neural networks, only one of which innervates the muscles*, *J. Neurosci.*, 23 (2003), pp. 8911–8920.
- [29] J. C. WEEKS, *Neuronal basis of leech swimming: Separation of swim initiation, pattern generation, and intersegmental coordination by selective lesions*, *J. Neurophys.*, 45 (1981), pp. 698–723.
- [30] D. E. WOOD, Y. MANOR, F. NADIM, AND M. P. NUSBAUM, *Intercircuit control via rhythmic regulation of projection neuron activity*, *J. Neurosci.*, 24 (2004), pp. 7455–7463.